J. Adv. Model. Earth Syst., Vol. 3, Art. M06003, 23 pp.

Intercomparison of cloud model simulations of Arctic mixed-phase boundary layer clouds observed during SHEBA/FIRE-ACE

Hugh Morrison[1], Paquita Zuidema[2], Andrew S. Ackerman[3], Alexander Avramov[3,4], Gijs de Boer[5], Jiwen Fan[6], Ann M. Fridlind[3], Tempei Hashino[7], Jerry Y. Harrington[8], Yali Luo[9], Mikhail Ovchinnikov[6] and Ben Shipway[10]*

[1] National Center for Atmospheric Research, Boulder, CO, USA[#]
[2] Rosenstial School of Marine and Atmospheric Sciences, University of Miami, Miami, FL, USA
[3] NASA Goddard Institute for Space Studies, New York, NY, USA
[4] The Earth Institute, Columbia University, New York, NY, USA
[5] Lawrence Berkeley National Laboratory, Berkeley, CA, USA
[6] Pacific Northwest National Laboratory, Richland, Washington, USA
[7] University of Wisconsin - Madison, Madison, Wisconsin, USA, now at University of Tokyo, Tokyo, Japan
[8] Pennsylvania State University, State College, Pennsylvania, USA
[9] Chinese Academy of Meteorological Sciences, Beijing, China
[10] UK Met Office, Exeter, United Kingdom

Revised manuscript submitted to *JAMES*, 4 February 2011

An intercomparison of six cloud-resolving and large-eddy simulation models is presented. This case study is based on observations of a persistent mixed-phase boundary layer cloud gathered on 7 May, 1998 from the Surface Heat Budget of Arctic Ocean (SHEBA) and First ISCCP Regional Experiment - Arctic Cloud Experiment (FIRE-ACE). Ice nucleation is constrained in the simulations in a way that holds the ice crystal concentration approximately fixed, with two sets of sensitivity runs in addition to the baseline simulations utilizing different specified ice nucleus (IN) concentrations. All of the baseline and sensitivity simulations group into two distinct quasi-steady states associated with either persistent mixed-phase clouds or all-ice clouds after the first few hours of integration, implying the existence of multiple states for this case. These two states are associated with distinctly different microphysical, thermodynamic, and radiative characteristics. Most but not all of the models produce a persistent mixed-phase cloud qualitatively similar to observations using the baseline IN/crystal concentration, while small increases in the IN/crystal concentration generally lead to rapid glaciation and conversion to the all-ice state. Budget analysis indicates that larger ice deposition rates associated with increased IN/crystal concentrations have a limited *direct* impact on dissipation of liquid in these simulations. However, the impact of increased ice deposition is greatly enhanced by several interaction pathways that lead to an increased surface precipitation flux, weaker cloud top radiative cooling and cloud dynamics, and reduced vertical mixing, promoting rapid glaciation of the mixed-phase cloud for deposition rates in the cloud layer greater than about $1-2\times10^{-5}$ g kg^{-1} s^{-1} for this case. These results indicate the critical importance of precipitation-radiative-dynamical interactions in simulating cloud phase, which have been neglected in previous fixed-dynamical parcel studies of the cloud phase parameter space. Large sensitivity to the IN/crystal concentration also suggests the need for improved understanding of ice nucleation and its parameterization in models.

DOI: 10.1029/2011MS000066

[#]National Center for Atmospheric Research is sponsored by the National Science Foundation

To whom correspondence should be addressed.
Hugh Morrison, National Center for Atmospheric Research, 3450 Mitchell Lane, Boulder, CO, 80307
morrison@ucar.edu

This work is licensed under a Creative Commons Attribution 3.0 License.

1. Introduction

The representation of clouds is a major challenge in numerical models of all scales. While the treatment of clouds in large-scale weather and climate models presents obvious challenges owing to the coarse resolution, there are still many uncertainties in high-resolution cloud models (i.e., with a horizontal grid spacing Δx of order 1 km or less). In particular, cloud microphysics and sub-grid scale turbulence are key challenges. Previous intercomparison studies of boundary layer stratocumulus using large-eddy simulation (LES) models subject to the same initial conditions and large-scale forcing have shown considerable spread in solutions (Moeng et al. 1996; Stevens et al. 2005; Klein et al. 2009). For example, an intercomparison of LES based on a marine stratocumulus case from the Dynamics and Chemistry of Marine Stratocumulus (DYCOMS-II) showed large spread among models in terms of liquid water path and various turbulence-related quantities. This spread was attributed to differences in numerics and subgrid mixing schemes, which strongly affect entrainment at cloud top (Stevens et al. 2005). Documenting and understanding differences and sources of uncertainty in these models is a critical first step toward determining the suitability of the results from such models for use in the development and evaluation of parameterizations in larger-scale models.

The Arctic presents unique challenges to modelers because of the frequent occurrence of cloud types and characteristics that are less common at lower latitudes (Curry et al. 1996). Furthermore, there has traditionally been a relative dearth of observations in this region. However, several field programs in recent years have begun to address this deficiency, including the 1994 Beaufort and Arctic Storms Experiment (Curry et al. 1997), 1997–1998 Surface Heat Budget of the Arctic Ocean Experiment (SHEBA, Uttal et al. 2002), the 1998 First International Satellite Cloud Climatology Project Regional Experiment – Arctic Clouds Experiment (Curry et al. 2000), the 2004 Mixed-Phase Arctic Cloud Experiment (M-PACE; Verlinde et al. 2007), the 2008 Indirect and Semi-Direct Aerosol Campaign (ISDAC; McFarquhar et al. 2011), and the ongoing ARM program site operating near Barrow, Alaska (Ackerman and Stokes 2003).

A key finding from these experiments is the frequency and persistence of supercooled liquid water and mixed-phase clouds, even at temperatures substantially below freezing (Curry et al. 2000; Intrieri et al. 2002; Korolev et al. 2003; Shupe and Intrieri 2004; Verlinde et al. 2007; de Boer et al. 2011; McFarquhar et al. 2011). The frequent occurrence of mixed-phase clouds has important implications for coupling with other components of the system. Mixed-phase clouds tend to be optically-thicker than clouds composed entirely of ice (Sun and Shine 1994; Shupe and Intrieri 2004; Shupe et al. 2006), resulting in considerably larger downwelling longwave radiative flux at the surface (e.g., Shupe and Intrieri 2004) and greater cloud top radiative cooling (e.g., Morrison and Pinto 2006). The impact of mixed-phase clouds on the surface energy budget in the Arctic is especially critical given the observed rapid decrease of sea ice extent and volume in recent years (e.g., Stroeve et al. 2007).

Numerous modeling studies have shown that the parameterization of microphysics is a key in simulating Arctic mixed-phase clouds (e.g., Harrington et al. 1999; Jiang et al. 2000; Morrison et al. 2003; Morrison and Pinto 2005; Sandvik et al. 2007; Prenni et al. 2007; Luo et al. 2008a; Fan et al. 2009). In particular, several studies have documented strong sensitivity of these clouds to ice particle or ice nucleus (IN) concentrations (e.g., Pinto 1998; Harrington et al. 1999; Jiang et al. 2000; Morrison et al. 2003; Prenni et al. 2007; Luo et al. 2008b; Solomon et al. 2009; Avramov and Harrington 2010). In several of these studies, mixed-phase clouds could only be maintained by decreasing concentrations of IN far below typical values observed in mid-latitudes (Jiang et al. 2000; Morrison and Pinto 2006; Prenni et al. 2007; Solomon et al. 2009). Some observations have suggested relatively low concentrations of IN in the Arctic (Bigg 1996; Rogers et al. 2001; Prenni et al. 2007; Prenni et al. 2009). However, such low values are in some cases inconsistent with observed crystal concentrations, suggesting the existence of nucleation modes not typically captured by IN measurements (Fridlind et al. 2007; 2011). In models that are able to maintain persistent mixed-phase clouds, a small increase in the IN/crystal concentration (within uncertainty of observations) often leads to rapid dissipation of liquid water (e.g., Harrington et al. 1999; Morrison et al. 2005a; Prenni et al. 2007; Solomon et al. 2009; Avramov and Harrington 2010). The degree of this sensitivity depends on other aspects of ice microphysics, such as ice particle habit and fallspeed (Avramov and Harrington 2010). Models have shown less sensitivity to the initial IN concentration when it is treated prognostically rather than diagnostically because of rapid depletion of IN within the cloud layer (Harrington and Olson 2001; Morrison et al. 2005a; Fridlind et al. 2007; 2011). Several studies have suggested the importance of cloud dynamics in maintaining mixed-phase clouds, with a balance between production of liquid water from upward motion and its depletion via the Bergeron-Findeisen process[1] (Mazin 1986; Rauber and Tokay 1991; Harrington et al. 1999; Korolev and Isaac 2003; Korolev 2007; Korolev and Field 2008).

The Global Energy and Water Experiment Cloud Systems Study (GCSS) project (Randall et al. 2003)) recognized the

[1] The Bergeron-Findeisen process is the preferential growth of ice by vapor deposition and evaporation of liquid water due to the lower equlibrium vapor pressure of ice. As described by Korolev (2007), under certain thermodynamic conditions ice deposition in mixed-phase clouds does not occur by evaporation of liquid. However, in this instance ice deposition still reduces the growth rate of liquid drops from what it would otherwise be. To avoid confusion, hereafter we use the term "ice deposition" to describe the growth of ice at the expense of liquid water through deposition, either via the Bergeron-Findeisen process, or indirectly via the reduction of drop growth rates.

importance of polar clouds and their interaction with other components of the climate system by forming the Polar Cloud Working Group (PCWG). A key GCSS activity is the model intercomparison study in which observed cases are simulated by cloud-resolving models (CRMs), single-column models (SCMs), or LES models and results compared to observations. This effort synthesizes CRM and LES results to help guide development and evaluation of parameterizations for large-scale models, with the ultimate goal of improving the representation of important cloud types in climate and weather models.

Under the auspices of the GCSS PCWG and the ARM program, the intercomparison studies of Klein et al. (2009) and Morrison et al. (2009a) documented the performance of several SCMs, CRMs, and LES for cases of Arctic mixed-phase boundary layer stratocumulus and multi-layer mixed-phase stratus. They found a large spread in key simulated quantities such as liquid and ice water paths and surface radiative fluxes. Results from the CRMs and LES were in general no better than the SCMs when compared to available observations. There was some indication of improved results in models using more detailed microphysics schemes, but there was considerable scatter among models with a given type of microphysics scheme and thus the significance of this trend was not clear. While ice microphysics appeared to be important in explaining biases in liquid water path (LWP) there was no clear relationship between LWP and ice crystal concentration (N_i) among the models. This result conflicts with previous studies that showed a strong sensitivity to IN concentration or N_i for a given model (e.g., Pinto 1998; Harrington et al. 1999; Jiang et al. 2000; Morrison et al. 2003; Prenni et al. 2007; Avramov and Harrington 2010) and it suggested the need for a more detailed analysis of microphysical process rates and more constrained frameworks to better understand causes of the large model discrepancies.

In the current study, we use data from SHEBA/FIRE-ACE and return to the intercomparison framework to evaluate CRM simulations and LES of the Arctic mixed-phase stratus-topped boundary layer. This work represents a joint effort under the auspices of the GCSS PCWG and Seventh World Meteorological Organization (WMO) Cloud Modeling Workshop (Morrison et al. 2009b). The approach is similar to previous intercomparison studies in which models are subject to the same initial conditions and large-scale forcing. The case study here differs in many key ways from the Arctic mixed-phase cloud cases in Klein et al. (2009) and Morrison et al. (2009a); these differences are detailed in section 2b. We also follow the recommendation of Klein et al. (2009) by utilizing a more constrained modeling framework in which N_i is essentially held fixed during the simulations. The current study further extends the work of Klein et al. (2009) and Morrison et al. (2009a) by including detailed analyses of microphysical process rates and budgets, as well as sensitivity tests to elucidate how models respond to changes in the specified IN concentration/N_i.

Broadly, the goals of this study are 1) to document this case, which provides a framework for additional modeling studies investigating Arctic mixed-phase cloud processes; 2) to document the spread of CRM and LES results and elucidate causes of differences in the simulations, especially in terms of interactions between microphysics, radiation, and dynamics; and 3) to determine the generality of previously reported sensitivities to IN among models, by exploring these sensitivities within a common framework.

2. Case description

SHEBA centered on a heavily-instrumented icebreaker ship frozen into the sea ice in the Beaufort Sea during fall 1997 and allowed to drift with the pack ice for one year (Uttal et al. 2002). During May and July 1998, the National Center for Atmospheric Research C-130 aircraft gathered measurements near the SHEBA site as part of FIRE-ACE (Curry et al. 2000). In May 1998 the SHEBA site was located near 76°N, 165°W. The case used here is derived from observations gathered from 1200–2400 UTC on 7 May, 1998. The cloud system consisted of a persistent mixed-phase boundary layer (BL) cloud that precipitated ice to the surface in the form of light snow showers.

2.1 Instrumentation

Ground-based instrumentation at SHEBA was used to remotely sense clouds. Radar reflectivity was provided by Millimeter Wavelength Cloud Radar (MMCR). LWP was retrieved from microwave radiometer measurements, making use of an estimated cloud temperature [Y. Han, unpublished data, see Zuidema et al. (2005) and Han and Westwater (1995) for further details]. The retrieval error is estimated at 10 g m^{-2} at 2-min time resolution. These LWPs are typically slightly higher, by $\sim$ 5 g m^{-2}, than those retrieved from an Atmospheric Emitted Radiance Interferometer (David Turner, personal communication). Ice water content (IWC) retrievals from the MMCR reflectivity were based on a mass-size relationship for radiating assemblages of plates (Mitchell et al. 1990). This relationship provided reasonable agreement between calculated and observed reflectivities (Fridlind et al. 2011), and is consistent with particle habits observed directly by imaging probes. Rawinsondes were launched at 1115, 1730, and 2335 UTC 7 May providing profiles of temperature and relative humidity (RH).

Two-dimensional cloud (2D–C) and precipitation (2D–P) optical array probes were included on the C-130 for the FIRE-ACE research flights. Details of the processing technique and analysis of the 2D-C and 2D-P measurements are found in Morrison et al. (2011). The Cloud Particle Imager (CPI) was also included on these flights and was used for manual classification of particle habit and estimate of the phase (Lawson and Zuidema 2009). Additional instruments were included on the C-130 for measuring bulk liquid water

mass content (King probe), sizing of particles between 2 and 47 μm (forward scattering spectrometer probe, FSSP-100), and Continuous Flow Diffusion Diffusion Chamber (CFDC) for IN concentrations (Rogers et al. 2001). See Zuidema et al. (2005) and Lawson and Zuidema (2009) for a detailed discussion of the processing methods and measurement uncertainties associated with these instruments.

2.2 Overview

Observations for the case are detailed in Zuidema et al. (2005), Morrison et al. (2011), and Fridlind et al. (2011); a brief description is given here. The synoptic situation consisted of a broad high-pressure region centered ~ 300 km south of the SHEBA site (Fig. 1). The National Centers for Environment Prediction/National Center for Atmospheric Research (NCEP/NCAR) Reanalysis showed large-scale subsidence of about 100 Pa h^{-1} at 850 hPa. The boundary layer depth had decreased from previous days in response to the strengthening high pressure and increased subsidence. Temperatures of the mixed-phase layer were between −18° and −22°C. Time-height plots of MMCR reflectivity indicate a persistent BL cloud deck with precipitation likely reaching the surface (Fig. 2). Note that the sharp decrease of reflectivity below 150 m in Fig. 2 is an artifact due to the MMCR "dead zone" where the receiver is blanked to avoid damage to the electronics from the transmitted pulse; surface reports suggest that light ice precipitation reached the surface, although the SHEBA Project Office snow gauge recorded no measurable precipitation during the period. The presence of MMCR reflectivities exceeding −20 dBZ at these temperatures is strongly suggestive of ice, while the lidar and LWP retrievals indicate the presence of liquid. The close proximity of liquid and ice particles within the cloud layer and ice precipitation beneath the layer were also indicated by in-situ observations from aircraft.

Profiles of temperature from sonde measurements (Fig. 3a) indicate a relatively well-mixed BL from the surface to near cloud top, presumably driven by cloud top radiative cooling given the small surface buoyancy flux and fairly weak shear. At the top of the BL there is a temperature inversion of 5–6 K over a depth of about 70 m. The depth of the BL (as determined by the altitude of the base of the temperature inversion) decreased from about 630 m to 400 m between the 1115 and 2335 UTC soundings (Fig. 3a). This was associated with a decrease in LWP from about 40 to 8 g m^{-2} and increase in BL temperature of about 1.5 K, and is consistent with the decrease in vertical extent of hydrometeors indicated by MMCR (Fig. 2). Retrieved ice water path (IWP) was generally between 0.5 and 2 g m^{-2}.

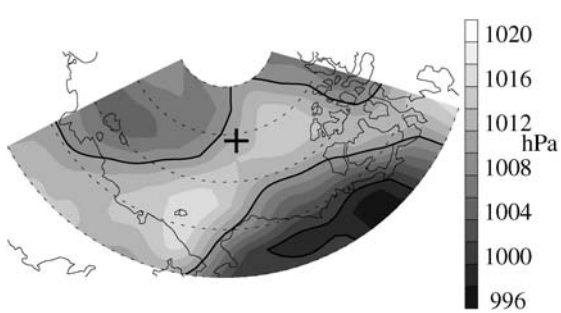

Figure 1. Sea level pressure from NCEP/NCAR reanalysis for 7 May, 1998. Location of the SHEBA site is indicated by +.

Ascent and descent profiles within the cloud and horizontal legs in ice precipitation beneath the mixed-phase layer were sampled by the C-130 between about 2200 and 2400 UTC. Liquid water content was less than 0.08 g m^{-3} and generally increased with height within the mixed-phase layer except near cloud top (see Fig. 5 in Zuidema et al. 2005). Measurements from the FSSP in the mixed-phase layer suggested droplet concentrations between about 200 and 230 cm^{-3}. CPI imagery indicated the prevalence of single plates, side planes, and radiating assemblages of plates, with little evidence for riming or aggregation (Morrison et al. 2011; Fridlind et al. 2011). Lack of aggregation is also suggested by particle size distributions from 2DC/2DP indicating few particles larger than 2−3 mm. Size distributions did not vary much with height, suggesting the role of vertical mixing of ice particles (Morrison et al. 2011). Values of N_i were low, with a mean N_i of particles larger than 100 μm of 0.44 L^{-1} (averaged over 10 s data points with IWC > 0.0001 g m^{-3}).

This case differs in several key ways from the mixed-phase boundary layer stratocumulus observed during M-PACE that formed the basis of the intercomparison study of Klein et al. (2009). First, total surface heat fluxes were estimated to be more than an order of magnitude smaller over the mostly sea ice-covered surface at SHEBA than over the open ocean near Barrow during M-PACE. Large surface heat fluxes combined with low-level shear led to formation of roll stratocumulus during M-PACE, with more vigorous cloud dynamics and greater amounts of cloud liquid and ice than the SHEBA case. The SHEBA case also had higher aerosol loading and droplet concentrations than M-PACE, and cloud temperatures were 5° to 7° C lower. Finally, microphysical characteristics differed substantially between the SHEBA and M-PACE cases. For the SHEBA case, there was limited riming and aggregation, with few crystals larger than 2−3 mm observed. In contrast, M-PACE featured large aggregates exceeding 6−8 mm in size, numerous dendrite crystals, and evidence of riming. The relative simplicity of the SHEBA case in terms of the microphysics makes it particularly well-suited as the basis for a model intercomparison.

3. Model descriptions

Six CRM and LES models participated in this study. Table 1 encapsulates relevant characteristics of these models. The models are only briefly described here; for more detailed

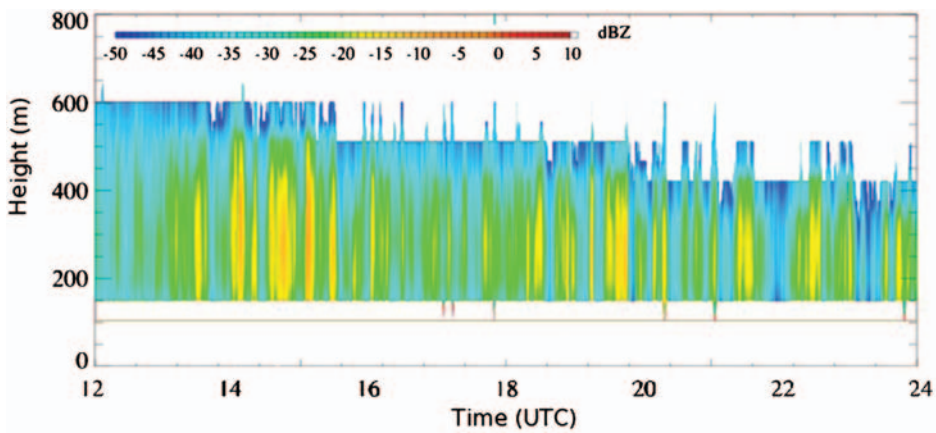

Figure 2. Time-height plot of the SHEBA MMCR reflectivity on 7 May, 1998.

description we refer readers to the references given in Table 1. In terms of their configurations for this study, four of the models (RAMS-CSU, UCLA-CAMS, SAM-SBM, UW-NMS) are two-dimensional (2D) and two (DHARMA, METO) are three-dimensional (3D). There is a wide range of horizontal and vertical resolutions and domain sizes. Horizontal grid spacing ranges from 50 to 2000 m, with the number of vertical levels within the BL ranging from 11 to 45. The horizontal domain length ranges between 3.2 and 256 km.

Since parameterization of microphysics is believed to be a key in simulating Arctic mixed-phase BL clouds, details of the microphysics schemes in the models are also provided in Table 1. All of the models here utilize relatively complex microphysics parameterizations. Three models (UW-NMS, SAM-SBM, DHARMA) use detailed bin microphysics, while the other three (RAMS-CSU, UCLA-CAMS, METO) use two-moment bulk microphysics schemes. Within a given category (bin or two-moment bulk), details of the approaches vary considerably. The number and type of predicted variables vary in the two-moment bulk schemes, although all of these schemes separately prognose variables for cloud liquid water and ice and liquid and ice precipitation. All models except METO and RAMS-CSU include coupling of droplet activation with the aerosols described in the Appendix.

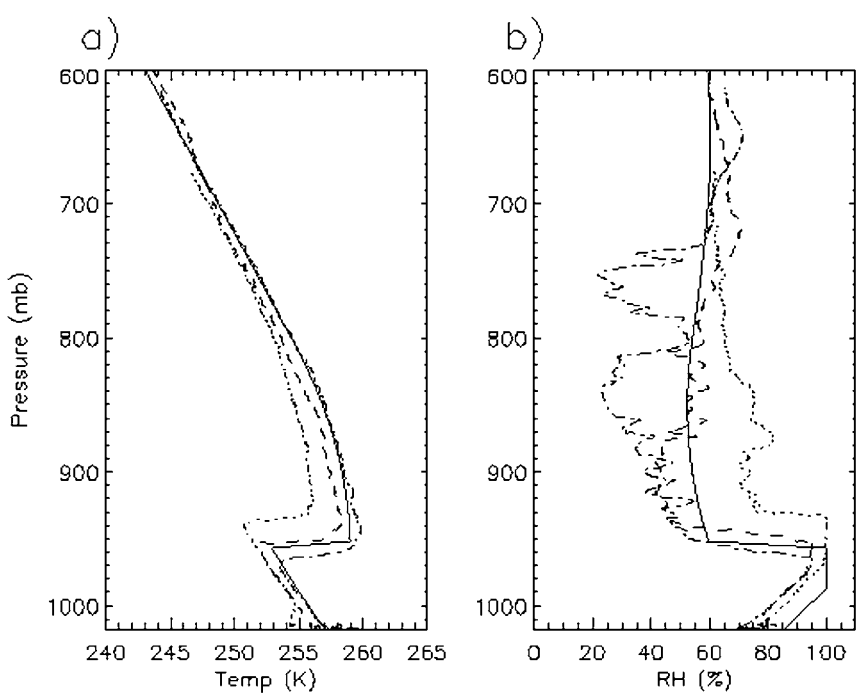

Figure 3. Observed a) temperature and b) relative humidity (RH) from sondes launched at 1115 (dotted), 1730 (dash), and 2335 (dot-dash) UTC 7 May. The initial profiles used in the model simulations are shown by the solid line.

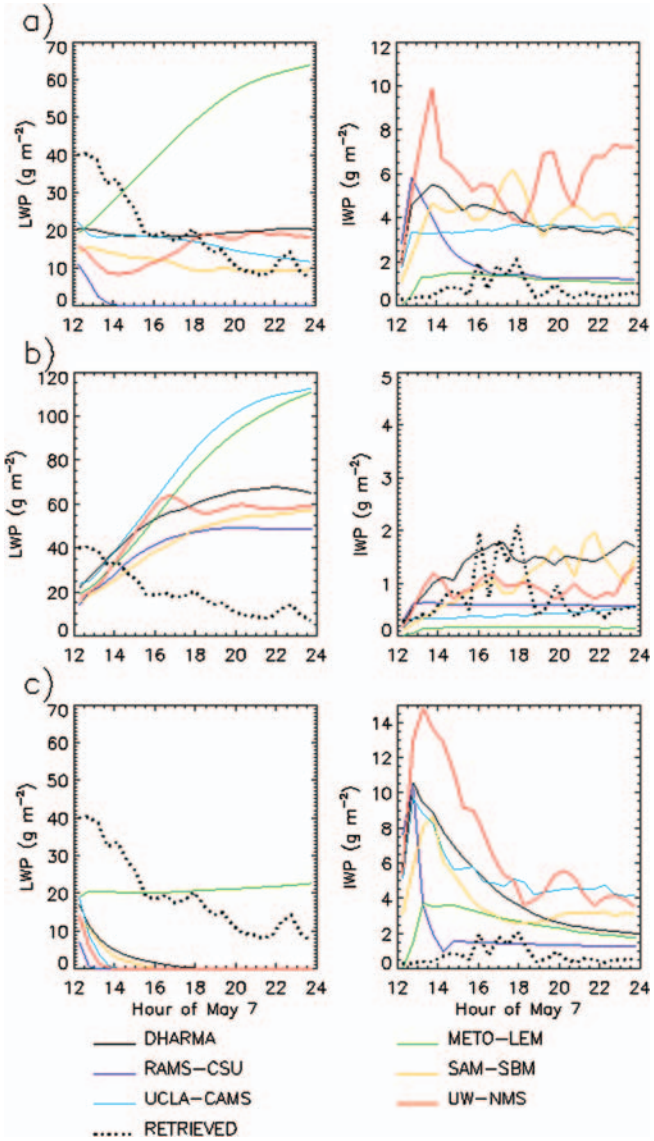

Figure 4. Timeseries of modeled and retrieved LWP and IWP for a) BASE, b) LOWNI, and HIGHNI.

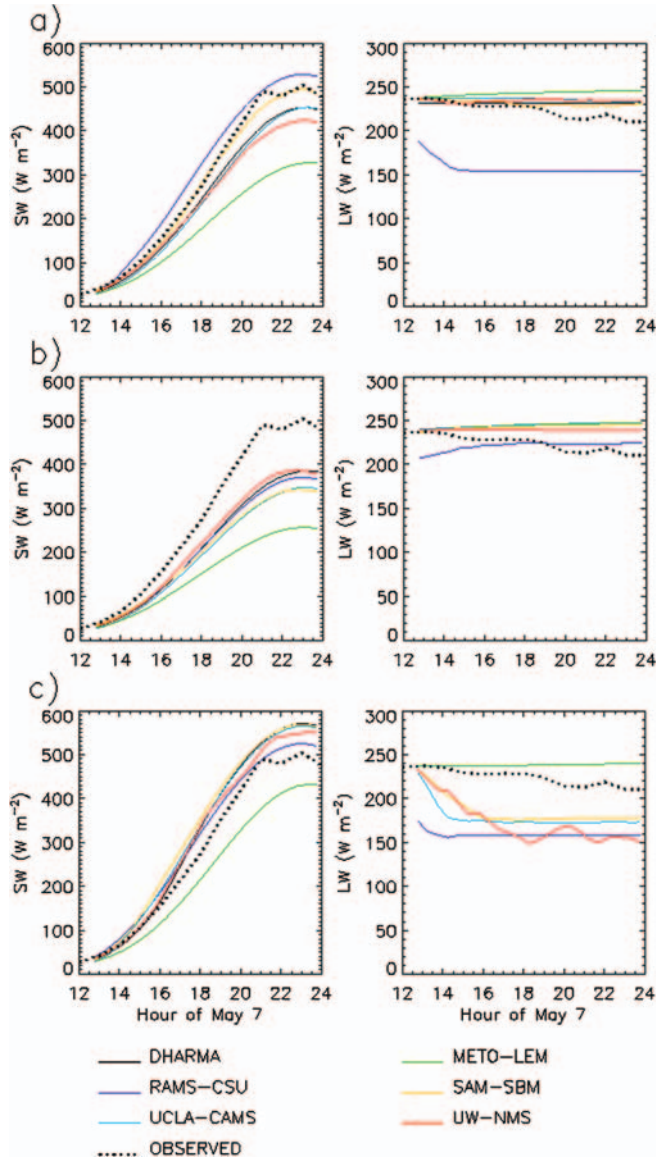

Figure 5. Timeseries of modeled and observed surface downwelling shortwave (SW) and longwave (LW) radiative fluxes for a) BASE, b) LOWNI, and c) HIGHNI.

4. Experimental setup

Initial and forcing conditions for this case are similar to the setup for the mixed-phase stratocumulus intercomparison case from Klein et al. (2009). The initial conditions for all models consist of a cloud-topped, well-mixed boundary layer (BL) with a height of about 500 m, based on sondes launched at 1115, 1730, and 2335 UTC 7 May. Here, we utilize somewhat idealized initial conditions corresponding with an adiabatic liquid cloud and time-averaged large-scale forcing designed to simplify the model setup and produce quasi-steady thermodynamic profiles above the BL. Simulations are integrated for 12 h starting 1200 UTC 7 May, 1998. A detailed description of the experimental setup, initial and surface conditions, and large-scale forcing is given in the Appendix.

Studies have shown that representation of ice nucleation is important in simulating Arctic mixed-phase clouds (e.g., Harrington et al. 1999; Morrison et al. 2005a; Fridlind et al. 2007; Prenni et al. 2007; Luo et al. 2008a,b; Fan et al. 2009). Since model parameterizations of ice nucleation vary widely and this process remains relatively poorly constrained by observations and theory (cf., Fridlind et al. 2007), we decided to constrain nucleation and hence N_i in the models and focus instead on differences in the representation of other processes. Otherwise, it was thought that different nucleation parameterizations in the models might dominate the results. Constraining N_i in this manner is a unique aspect of this study, although it was suggested by Klein et al. (2009).

Table 1. Summary of the participating models.

Model	*Investigator(s) and model reference*	*Cloud microphysics*	*Prognostic cloud variables*	*Dimensionality, Horizontal gridspacing, domain size*	*# of vertical levels in the BL**
DHARMA	Ann Fridlind Andy Ackerman *Ackerman et al. (2004)*	bin microphysics *Ackerman et al. (1995)* *Fridlind et al. (2007)*	32 liquid and 32 ice bins	3D 50 m 3.2 km × 3.2 km	43
METO	Ben Shipway *Shutts and Gray (1994)*	double moment *Ferrier (1994)*	q_l, q_r, q_i, q_s, q_a N_i, N_s, N_g	3D 50 m 6.4 km × 6.4 km	45
UW-NMS	Gijs de Boer Tempei Hashino *Tripoli (1992)*	bin microphysics, SHIPS, *Hashino and Tripoli (2007; 2008)*	40 liquid and 20 ice bins	2D 100 m 15 km	20
RAMS-CSU	Alex Avramov Jerry Harrington *Cotton et al. (2003)*	double moment *Meyers et al. (1997)*	q_l, q_r, q_i, q_s, q_a, q_g N_r, N_i, N_s, N_a, N_g	2D 1 km 150 km	13
SAM-SBM	Jiwen Fan Mikhail Ovtchinnikov *Khairoutdinov and Randall (2003)* *Fan et al. (2009)*	bin microphysics*Khain et al. (2004)*	33 bins each for liquid drops, ice crystals, snowflakes, graupel, and hail/frozen drops	2D 100 m 12.7 km	29
UCLA-CAMS CRM	Yali Luo *Krueger (1988)* *Luo et al. (2008)*	double moment *Morrison et al. (2005b)*	q_l, q_r, q_i, q_s, N_l, N_r, N_i, N_s	2D 2 km 256 km	11

*Number of vertical levels in the BL is defined here in terms of the initial BL height.

For this study, ice nucleation in all models is treated diagnostically such that if N_i falls below the specified IN concentration, N_{IN}, it is nudged upward toward N_{IN} (when ice supersaturation exceeds 5%). This is done by

$$\left(\frac{\partial N_i}{\partial t}\right)_{nuc} = \max\left(0, \frac{N_{IN} - N_i}{\Delta t}\right), S_i \geq 5\% \qquad \left(\frac{\partial N_i}{\partial t}\right)_{nuc} = 0, S_i < 5\% \tag{1}$$

where S_i is the ice supersaturation and Δt is the model time step. In this setup, the only process that can increase N_i above the value of N_{IN} is convergence due to differential sedimentation (assuming continuity of the flow field), but this has little impact in the simulations here. Thus, in practice N_i is approximately constant and equal to the specified N_{IN} in all simulations using (1). For the bin schemes, nucleated ice particles are added to either the smallest one or two size or mass bins. For the bulk schemes, nucleation of new particles increases the bulk ice mass, assuming an initial ice particle size that is 10 μm or less.

The actual N_i is uncertain because of difficulties in measuring ice particles smaller than about 100 μm given the available instrumentation (Morrison et al. 2011; Fridlind et al. 2011). For the baseline simulations, we assume that $N_{IN} = 1.7\ \mathrm{L}^{-1}$ based on an average of CFDC measurements of IN made above the boundary layer under in-cloud conditions of temperature and supersaturation (Rogers et al. 2001). This is about 4 times the observed N_i for crystals larger than 100 μm. We utilize this approach because of the uncertainty in concentrations of small ice particles and suggestions that reliably-measured N_i in Arctic mixed-phase boundary layer clouds often roughly match IN concentrations above cloud top (Prenni et al. 2009). On the other hand, Fridlind et al. (2011) found that such IN concentrations are insufficient to explain observed ice crystal spectra for the 7 May SHEBA case based on LES results and theoretical arguments if entrainment is the dominant controlling factor providing a source of IN to the BL. Using their prognostic approach for IN, they had to increase the mean above-cloud N_{IN} active under in-cloud conditions by more than an order of magnitude to produce realistic ice size spectra, indicating that N_{IN} measured by the CFDC under cloud-top conditions could be insufficient to explain observed ice crystal spectra. To avoid these complications, we assume the diagnostic value of $N_{IN} = 1.7\ \mathrm{L}^{-1}$ without regard to any specific mode of nucleation, and acknowledge that this choice for N_{IN} is not well constrained by observations. To explore sensitivity to changes in this parameter, sensitivity tests were run with N_{IN} modified from the baseline value. These tests are described in section 6.

5. Baseline results

5.1 Liquid and ice water paths and microphysics

Although all models produce a horizontally-extensive BL cloud, there are substantial differences in terms of the cloud, thermodynamic, and dynamical quantities. Time evolution of horizontally-averaged LWP and IWP for the baseline simulations (BASE) and retrievals is shown in Fig. 4a. RAMS-CSU produces rapid glaciation of liquid water within the first two hours, while METO produces a steady increase of LWP to values larger than 60 g m^{-2} by the end of the integration at 2400 UTC 7 May. An additional simulation using METO but with the Ferrier (1994) microphysics scheme replaced by the two-moment scheme of Morrison

et al. (2009c) reproduces general features of the baseline METO run, although LWP is lower and IWP somewhat higher. The other models produce results that are grouped more closely together, with a quasi-steady LWP between 10 and 20 g m^{-2}. The models also exhibit large differences in IWP. Interestingly, RAMS-CSU and METO, with the lowest and highest LWP, respectively, both produce IWPs of about 1 g m^{-2} after 1600 UTC. The other models produce larger IWPs that range between about 3 and 8 g m^{-2}. Retrieved IWPs are generally smaller than the modeled values, ranging from about 0.5 to 2 g m^{-2} but typically less than 1 g m^{-2}. An overprediction of ice is consistent with radar reflectivities that are generally larger than observed for the models that reported this quantity, except for METO. The cause of the excessive LWP and IWP in most simulations compared to retrievals is unknown but may be due to shortcomings in the specified N_{IN} or large-scale forcing, among other factors. Fridlind et al. (2011) were able to reproduce observed conditions for the last two hours of this case when using reduced large-scale advective forcing of water vapor and reducing N_{IN} from 1.7 to 0.3 L^{-1} in the diagnostic approach to ice nucleation specified following Eq. (1).

Mean ice particle size for particles larger than 100 μm ranges from about 250 to 900 μm in ice precipitation below the simulated cloud layer, and decreases with height in the cloud layer. The observed value is between about 300 to 800 μm and exhibits considerable spatial and temporal variability (Morrison et al. 2011). Larger values of IWP than retrieved are consistent with simulated N_i that are larger than observed; concentrations of particles larger than 100 μm are up to about 4 times larger than the mean observed value of 0.44 L^{-1} from 2DC/2DP. Droplet concentrations in the simulations that predict this quantity are generally between 160 and 220 cm^{-3}, which is roughly consistent with observations. The models are not particularly sensitive to changes in the CCN and hence droplet concentrations (see Appendix).

5.2 Surface radiative fluxes

Given the generally larger mass and smaller effective radii of liquid droplets relative to ice, differences in horizontally-averaged surface downwelling shortwave (SW) and longwave (LW) radiative fluxes among the models (Fig. 5a) mostly reflect differences in LWP. In particular, RAMS-CSU produces the largest SW and smallest LW since it has the smallest LWP, while the opposite is true for METO since it has the largest LWP. LW is only about 15 W m^{-2} larger in METO than the models with LWP between 10 and 20 g m^{-2}, despite the much greater LWP in this simulation, since clouds emit as near-blackbodies for LWP greater than about 30 g m^{-2} (Shupe and Intrieri 2004). Most of the simulations have somewhat smaller SW and larger LW compared to observed values after about 2000 UTC, which is consistent with the general overprediction of LWP and IWP after this time (Fig. 4a).

5.3 Precipitation

Horizontally-averaged surface precipitation rates vary by about a factor of 5–7 among the simulations (Fig. 6). Precipitation is light and almost entirely ice phase; peak (liquid-equivalent) precipitation rates are less than 1 mm day^{-1} in all simulations. After an initial increase of precipitation corresponding with the spin-up of BL dynamics as well as ice formation and growth, surface precipitation rates reach quasi-steady values in all simulations. While large-scale and surface forcings are important constraints on surface precipitation, large differences in the quasi-steady precipitation rates among simulations suggest that different model representations of the BL and clouds exert a first-order control on precipitation rate for this case over the timescales examined.

5.4 Cloud and thermodynamic profiles

Horizontally-averaged profiles of liquid water potential temperature, θ_l, total water mixing ratio, q_t, liquid water mixing ratio, q_c, and ice mixing ratio, q_i, for the simulations averaged from simulation time t = 11.5 to 12 h (2330 to 2400 UTC) together with the specified initial profiles are shown in Fig. 7. Thermodynamic profiles in most simulations

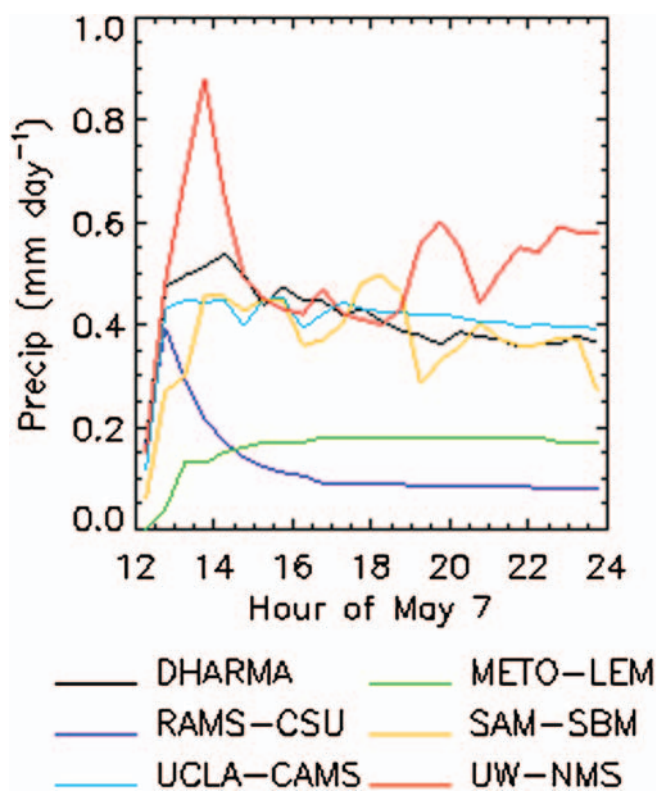

Figure 6. Timeseries of liquid-equivalent surface precipitation rates for BASE.

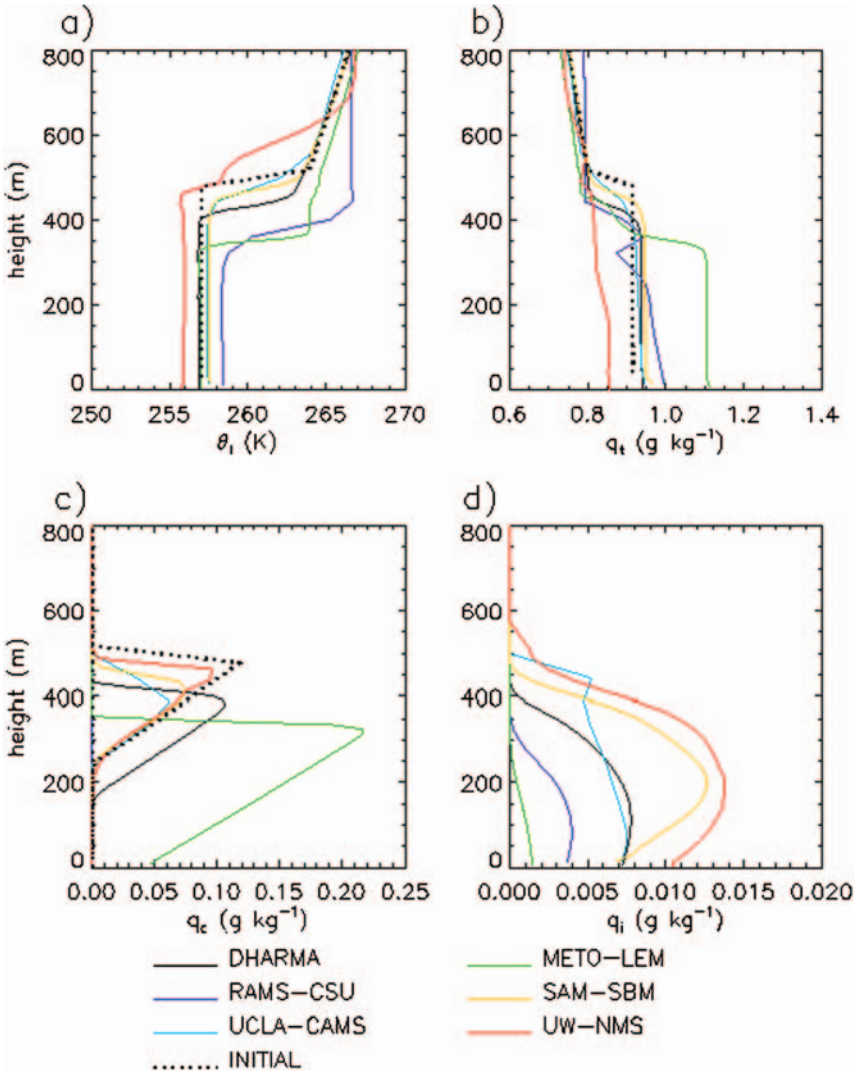

Figure 7. Horizontally-averaged vertical profiles for BASE of a) liquid water potential temperature, θ_l, b) total water mixing ratio, q_t, c) cloud water mixing ratio, q_c, and d) ice mixing ratio, q_i, averaged between t = 11.5 to 12 h. Specified initial profiles of θ_l, q_t, and q_c are also shown.

exhibit characteristics of a well-mixed, cloud-topped BL, with relatively constant θ_l and q_t, and q_c increasing with height. An exception is RAMS-CSU, which exhibits a profile of q_t that decreases sharply with height within the BL (Fig. 7b). The spread of θ_l in the BL among the simulations is about 2.5 K by the end of the integration (Fig. 7a). Differences in θ_l are mostly explained by differences in radiative cooling of the BL, which is described further below. Profiles of q_c and q_i vary widely among the models (Fig. 7c,d), consistent with the differences in LWP and IWP described above. In general, larger values of q_i (and surface precipitation rates) correspond with greater BL depth. METO and RAMS also tend to have the largest mass-weighted ice particle fallspeeds for a given q_i (not shown), which likely contributes to the small q_i in these simulations.

Horizontally-averaged vertical profiles of radiative heating rate averaged between t = 11.5 to 12 h for BASE are shown in Fig. 8a. Cloud top radiative cooling rates are mostly determined by the condensed water contents, which are dominated by liquid in most simulations. RAMS-CSU, which produces no liquid water after the first few hours of the simulation, has almost no cloud top radiative cooling.

An analysis of the water vapor budget sheds additional light on differences between the simulations. Horizontally-averaged vertical profiles of ice deposition and sublimation, condensation and evaporation of liquid droplets, large-scale 3D advection of q_v, the total tendency of q_v, and the residual term (calculated as the total q_v tendency minus ice deposition and sublimation, droplet condensation and evaporation, and large-scale advection) averaged from t = 11.5 to 12 h are shown in Fig. 9. The residual term is interpreted as the sum of the resolved and sub-grid vertical q_v flux convergence (referred to hereafter as the "q_v flux convergence").

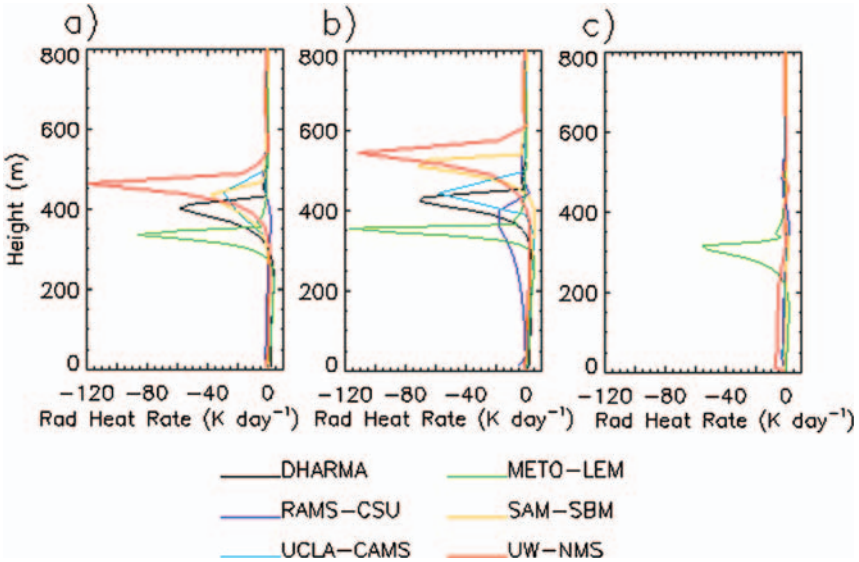

Figure 8. Horizontally-averaged vertical profiles of radiative heating rate averaged between t = 11.5 to 12 h for a) BASE, b) LOWNI, and c) HIGHNI.

The q_v budget in most simulations reflects primarily a balance between condensation (evaporation) and q_v flux convergence (divergence). Ice deposition and sublimation is a relatively small net sink for q_v, while large-scale 3D advection represents an overall source. The total tendency of q_v is generally much smaller than the other budget terms. In steady state, the vertical integral of ice deposition and sublimation is equal to the precipitation flux at the surface, which balances the surface turbulent moisture flux and vertical integral of the large-scale advective forcing of q_v. Some of the models experience a slow moistening (RAMS-CSU, METO) or drying (UW-NMS) of the q_v field (Fig. 9c), which reflects different surface precipitation rates (Fig. 6) and imbalances between the surface and large-scale advective forcing and the surface precipitation flux.

RAMS-CSU produces weakly negative q_v flux convergence in the upper one-fourth of the BL, and weakly positive q_v flux convergence at lower levels. These results, along with the sharp gradient of q_t within the BL (see Fig. 7b), indicate a lack of vertical mixing in this simulation. The gradient of q_t with $dq_t/dz < 0$ in RAMS-CSU can be mostly explained by the sedimentation of ice from the middle and upper part of the BL and its sublimation near the surface, resulting in a net downward transport of q_t. Weak vertical mixing is presumably due mostly to the lack of cloud top radiative cooling (Fig. 8a) and hence increased static stability of the upper BL. In contrast, the other simulations with sustained mixed-phase clouds generally have a stronger positive q_v flux convergence in much of the cloud layer (except in a narrow region right at the cloud top), and negative q_v flux convergence below. This profile of q_v flux convergence is consistent with an adiabatic, liquid topped well-mixed BL. Stronger vertical mixing in these runs appears to be driven by the greater rates of cloud top radiative cooling compared to RAMS-CSU (Fig. 8a), and is consistent with the relatively well-mixed q_t profiles seen in Fig. 7b.

Although RAMS-CSU produces an ice deposition rate between t = 11.5 to 12 h that is comparable to the other simulations (Fig. 9a), it is much larger in the mixed-phase layer at the start of the simulation. This is shown by a plot of ice deposition rate as a function of q_i for locations containing liquid water ($q_c > 0.001$ g kg^{-1}) during the first 6 h of integration (Fig. 10). In mixed-phase conditions, RAMS-CSU has an ice deposition rate that is about 3–5 times larger than the other models for a given q_i; it is smaller later in the simulation because of the subsequent reduction in RH which coincides with the dissipation of liquid water. It appears that large ice deposition rates produced by RAMS-CSU in mixed-phase conditions contribute to the rapid glaciation in this simulation through interactions with liquid water, radiation, and dynamics, as detailed in section 6. These large deposition rates are likely due to an oversimplification of crystal habit effects, as discussed by Avramov and Harrington (2010). We note that many other factors may also contribute to the divergence of solutions among the baseline simulations, including differences in horizontal and vertical grid spacings, model numerics, radiation codes, and treatment of sub-grid scale mixing, among others.

6. Sensitivity tests

In this section, we detail sensitivity tests that vary the specified N_{IN} used in Eq. (1). Note that since N_i is approximately fixed in time and space by the diagnostic approach used here, sensitivity to N_{IN} in this framework is analogous to sensitivity to N_i. In these tests, N_{IN} = 0.17 L^{-1} (LOWNI) or N_{IN} = 5.1 L^{-1} (HIGHNI), compared to the baseline

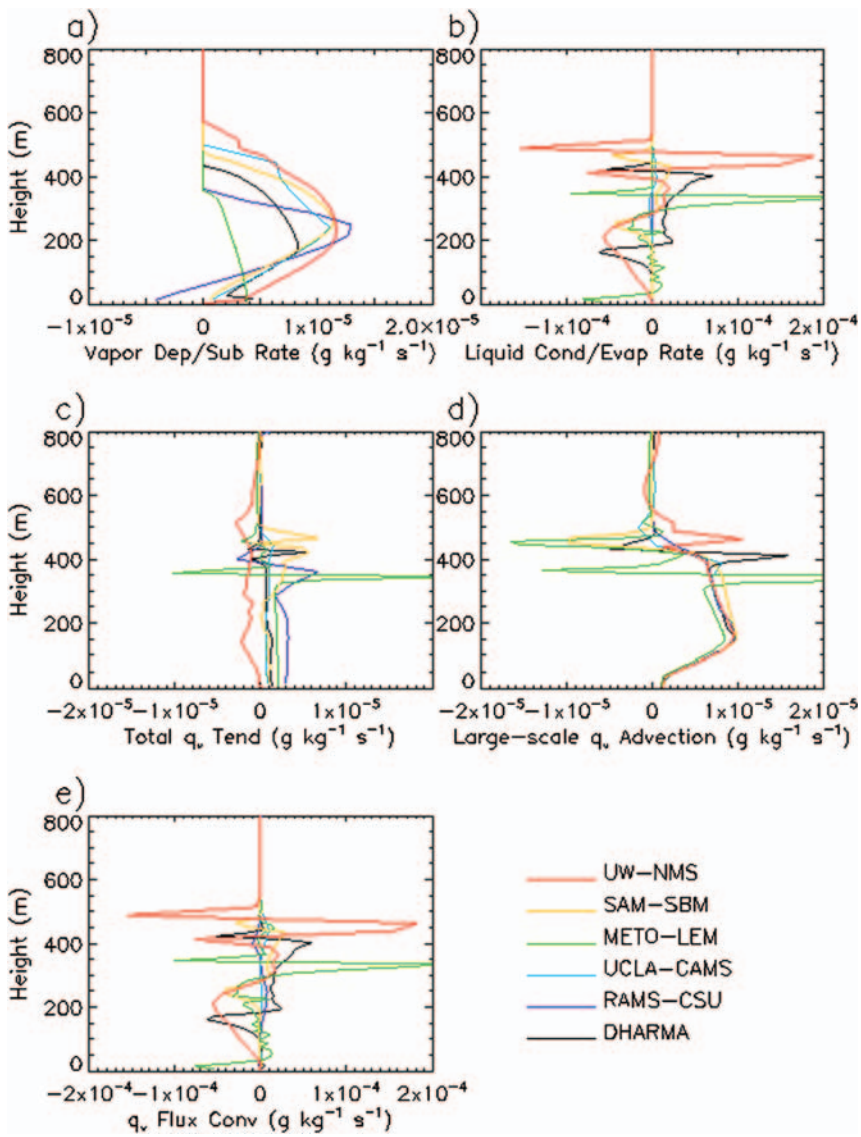

Figure 9. Horizontally-averaged vertical profiles of the q_v budget terms averaged between $t = 11.5$ to 12 h for BASE: a) ice deposition and sublimation, b) droplet condensation and evaporation, c) total q_v tendency, d) large-scale 3D advection, and e) sub-grid and resolved vertical q_v flux convergence (calculated as a residual, see text). Note different scales for the abscissa are used in the various plots.

$N_{IN} = 1.7$ L^{-1} (BASE). A third sensitivity test was also run with all ice microphysics shut off. However, these simulations are similar to LOWNI in terms of the liquid characteristics and interactions between the liquid microphysics, radiation, and dynamics, and are therefore not discussed. All other aspects of the model setup for the sensitivity tests are identical to the baseline simulations.

LWP and IWP for the sensitivity runs are shown in Figs. 4b,c, together with BASE in Fig. 4a. Overall, the LOWNI, BASE, and HIGHNI simulations cluster into two quasi-steady states within the first few hours of integration, corresponding with either persistent mixed-phase clouds or all-ice clouds after rapid glaciation of the liquid. LWP is highly sensitive to N_{IN} using the diagnostic approach for IN following Eq. (1) for the range of values tested; liquid water glaciates within the first few hours in all HIGHNI simulations except METO. For LOWNI, all models produce substantial liquid water over the duration of the simulations, notably including RAMS-CSU which did not sustain liquid water in BASE. IWP shows a generally nonmonotonic behavior with respect to changes in N_{IN}, with the smallest values in LOWNI, larger values in BASE, and similar or in many cases smaller values in HIGHNI (after the first 4–6 hours of the integrations) compared to BASE. This nonmonotonic behavior reflects drying of the BL and reduced ice growth rates in the HIGHNI simulations after glaciation. Surface precipitation increases with larger N_{IN} in the first 2–4 h of the simulations, but is fairly insensitive to N_{IN} after this time.

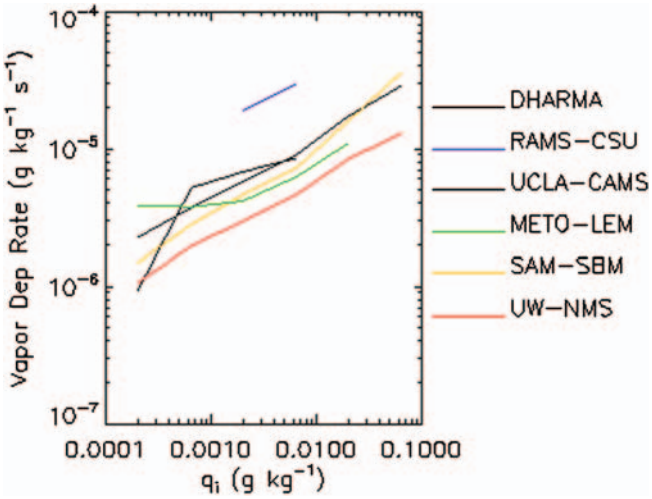

Figure 10. Mean ice deposition rate as a function of ice mixing ratio, q_i, for BASE, for the first 6 h of integration and locations with liquid water mixing ratio greater than 0.001 g kg^{-1}.

There is considerable sensitivity of the surface downwelling radiative fluxes and profiles of radiative heating to N_{IN} associated primarily with the large changes in LWP. Simulations that produce all-ice clouds have a downwelling LW flux about 50–70 W m^{-2} lower and downwelling SW flux about 100–200 W m^{-2} higher (at solar noon) than the simulations with persistent mixed-phase cloud (Fig. 5). Cloud top radiative cooling is also much smaller in the simulations with all-ice cloud (Fig. 8). However, there is substantial variability of cloud top radiative cooling even among the LOWNI simulations with substantial liquid water, which may reflect use of different radiation codes as well as other factors such as vertical grid spacing. For example, RAMS-CSU produces relatively weak cloud top cooling despite having a LWP near 50 g m^{-2}. To avoid this complication, future model intercomparisons of the Arctic mixed-phase cloudy BL may consider utilizing a simple parameterization of the radiative flux profiles as has been done in previous intercomparison studies of the warm stratocumulus-topped BL (Stevens et al. 2005).

The cloud dynamics exhibit large sensitivity to N_{IN}, which is not surprising given the large changes in cloud top radiative cooling and hence static stability of the upper BL. To illustrate this point, horizontally-averaged profiles of resolved turbulent kinetic energy (TKE) for LOWNI, BASE, and HIGHNI from SAM-SBM and DHARMA averaged between $t = 11.5$ and 12 h are shown in Fig. 11 (TKE is calculated using deviations of the resolved velocity components from their horizontal averages). Differences in TKE between LOWNI, HIGHNI, and BASE for a given model correspond closely with differences in the peak cloud top radiative cooling rates. TKE is substantially higher in the BL for the sustained mixed-phase clouds in LOWNI and BASE compared to the all-ice clouds in HIGHNI. TKE is only marginally higher in LOWNI than BASE, which is consistent with the relatively small differences in cloud top radiative cooling between these simulations (Fig. 8). While there are similar differences in TKE between all simulations with sustained mixed-phase cloud and those with conversion to all-ice cloud, there are large differences in TKE between different models, presumably due to the large differences in horizontal and vertical grid spacings and 2D versus 3D configurations, among other factors. For example, larger TKE in the 2D SAM-SBM compared to the 3D DHARMA is consistent with previous studies of the impact of dimensionality in simulations of radiatively-driven cloud-topped BL (Bretherton et al. 1999). Glaciation of the mixed-phase cloud due to increased N_{IN} is also associated with a tendency for reduced BL depth (as defined by the base of the temperature inversion), indicating reduced entrainment at

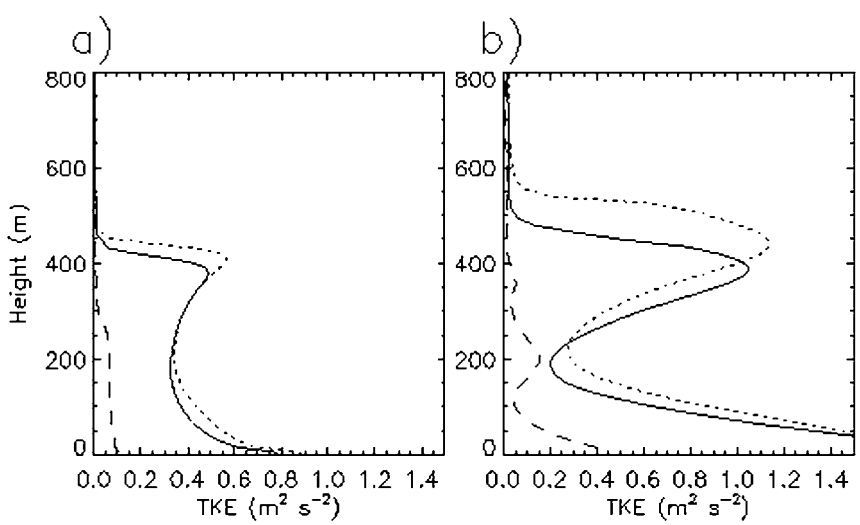

Figure 11. Vertical profiles of horizontally-averaged resolved turbulent kinematic energy (TKE) averaged between $t = 11.5$ and 12 h for BASE (solid), LOWNI (dotted), and HIGHNI (dash) from a) DHARMA and b) SAM-SBM.

the BL top. This is presumably a response to the large reduction of cloud top radiative cooling rates and hence vertical mixing associated with dissipation of liquid water, although widely-varying entrainment rates simulated by different models also likely reflect differences in numerics and subgrid scale schemes (Stevens et al. 2005).

Changes in the dynamics resulting from modification of N_{IN} have a major impact on vertical transport within the cloud layer. This finding is illustrated by horizontally-averaged vertical profiles of the q_v budget terms averaged between t = 11.5 and 12 h for LOWNI and HIGHNI (Figs. 12–13) along with BASE (Fig. 9). Overall, simulations cluster into two distinct groups in terms of the q_v budget, corresponding to the mixed-phase or all-ice states. In the HIGHNI and BASE simulations with rapid glaciation and conversion to all-ice cloud, the q_v flux convergence in the upper part of the BL is weakly negative, and weakly positive in the lower BL (Figs. 9e, 13e). Along with vertical profiles of q_t within the BL that exhibit a sharp decrease with height (not shown, except for RAMS-CSU in Fig. 7b for BASE), this indicates a lack of vertical mixing. As described previously, gradients of q_t develop mostly as a result of sedimentation and sublimation of ice near the surface. In contrast, the LOWNI, BASE, and HIGHNI simulations that sustain liquid water exhibit a positive vapor flux convergence in the cloud layer that largely balances the sink of q_v due to condensation, and relatively well-mixed profiles of q_t. This is consistent with the larger TKE in these simulations.

Magnitudes of the q_v flux convergence and condensation rate vary widely among the simulations. However, the peak values of q_v flux convergence and droplet condensation rate in the simulations that sustain liquid water are about 3 to 100 times larger than the ice deposition rate at the same vertical level, with the notable exception of the baseline

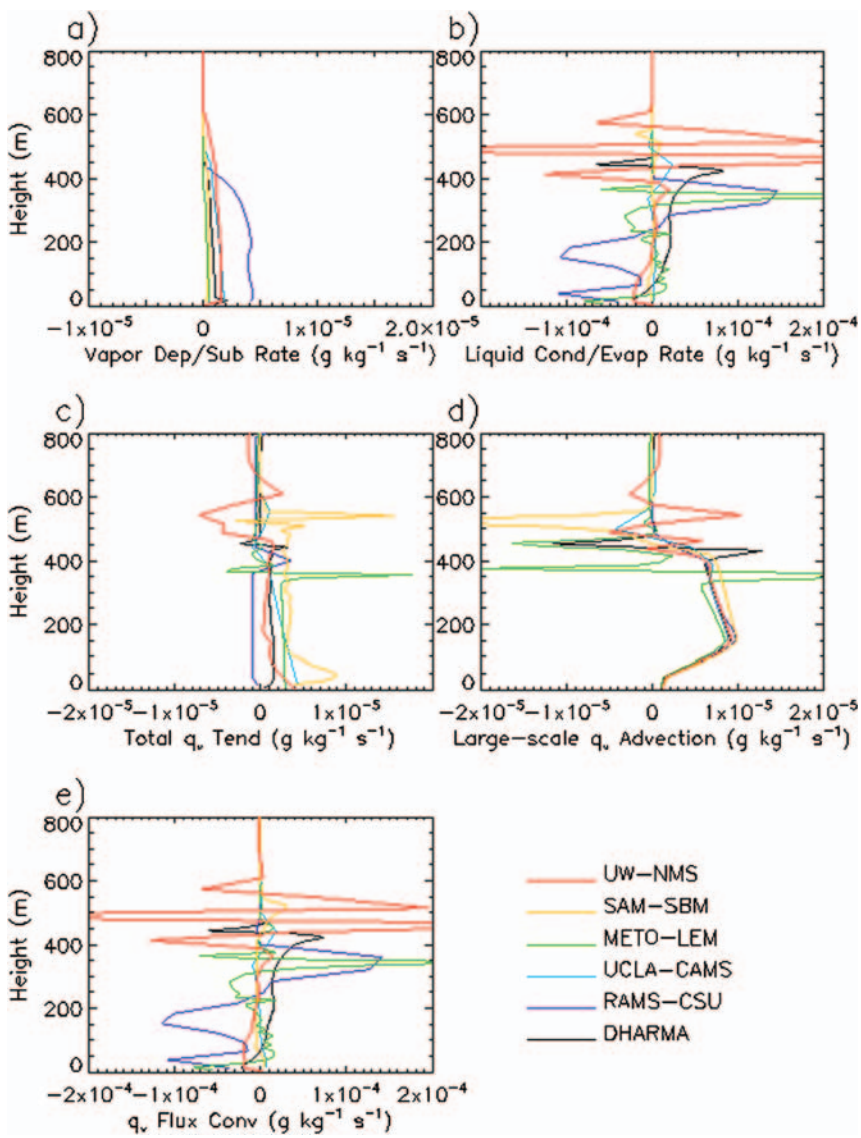

Figure 12. As in Figure 9, except for LOWNI.

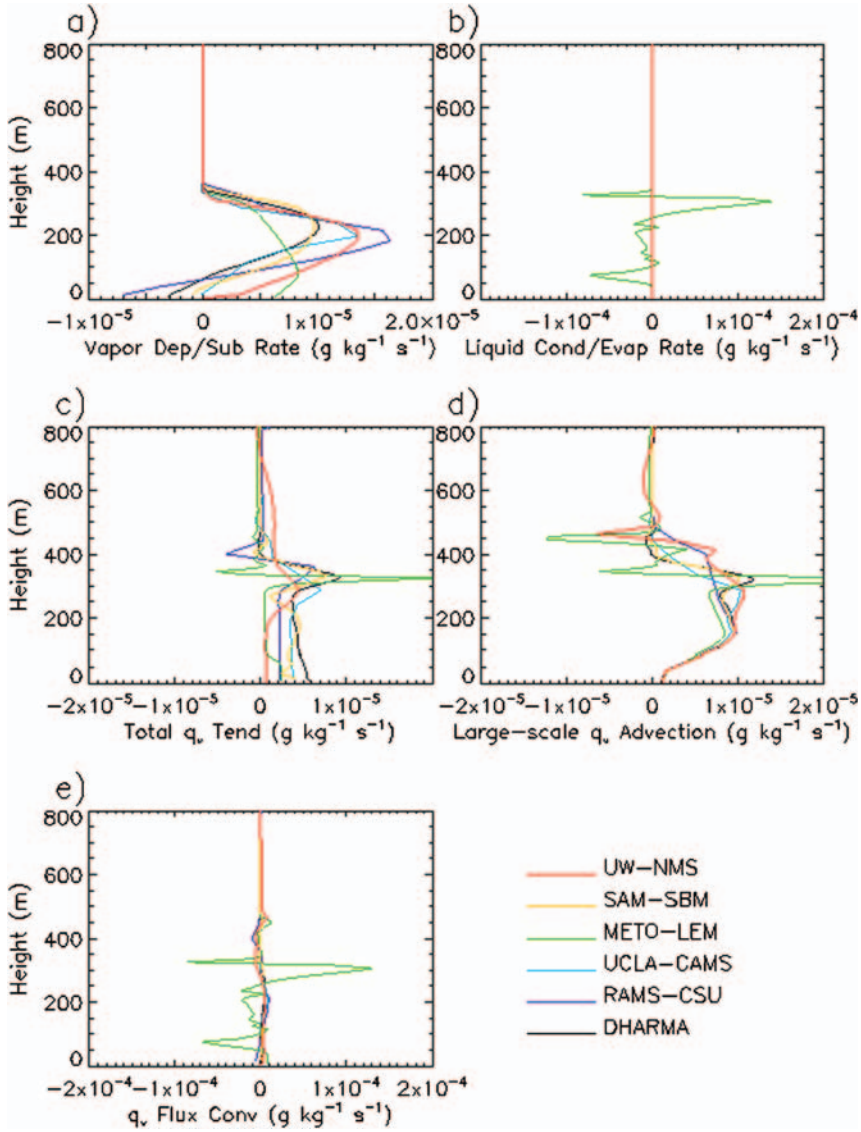

Figure 13. As in Figure 9, except for HIGHNI.

UCLA-CAMS run. In other words, the q_v flux convergence is large enough that it could support a positive condensation rate even if the deposition rate was increased by up to a factor of 3 or more in most of the simulations that are able to maintain liquid, all else being the same[2]. This implies that the *direct* impact of ice deposition on the maintenance of liquid water is limited. However, increased ice deposition rate has an important *indirect* impact on the maintenance of liquid water by influencing the surface precipitation flux, cloud top radiative cooling, and cloud dynamics. Three such interaction pathways are described below that act in concert to glaciate the cloud:

1) Greater ice deposition rates associated with increased N_{IN} lead to an increased precipitation flux at the surface, contributing both to a net warming (through latent heating) and drying (through the sink of water) of the BL and hence reduction of RH and erosion of liquid water. For example, a surface precipitation rate of 1 mm day^{-1} (a typical peak domain-average precipitation rate for the HIGHNI simulations) would result in complete dissipation of the initial liquid water in approximately 2.5 h assuming the BL remains well-mixed and neglecting changes in entrainment at the top of the BL. This time is similar to the actual glaciation timescale in the simulations with conversion to all-ice. However, in actuality it would take longer to completely glaciate the liquid water from this pathway alone because it takes 2–3 hours for the surface precipitation to spin up and reach values of $\sim$ 1 mm day^{-1}; furthermore, surface precipitation decreases after reaching its peak because of the warming and drying it induces.

[2] Increased ice deposition at the expense of condensation will also impact static energy due to the enthalpy of freezing, but this effect is small relative to other terms in the static energy budget and therefore does not change the overall argument presented here.

2) A reduction of liquid water as a result of increased ice depositional growth leads to weaker cloud top radiative cooling in simulations with increased N_{IN}, as discussed previously. This leads directly to warming of the BL and hence reduction of RH and further dissipation of liquid in simulations, representing a positive feedback. As an estimate, if the radiative flux divergence of the BL associated with the initial liquid water profile were removed, warming of the BL by roughly 4 K day^{-1} would occur. This process acting alone would lead to dissipation of the initial liquid water in about 12 h, again assuming the BL remains well-mixed and neglecting the impact of any changes in entrainment at the BL top. The tendency for reduced warming and drying as a result of reduced entrainment at the BL top with increased N_{IN} helps to counter this feedback; however, this is a second-order effect compared to the loss of radiative cooling associated with the liquid water.
3) Weaker cloud top radiative cooling associated with a reduction of liquid water in simulations with increased N_{IN} also leads to weaker cloud dynamics and hence vertical mixing, as the results discussed above imply. This leads to a decoupling of the mixed-phase layer from the sub-cloud environment, profiles of q_t that are no longer well-mixed and instead decrease with height, and reduced q_v flux convergence and condensation rate in the cloud layer. This in turn further reduces the liquid water, representing another positive feedback that accelerates glaciation. Once the peak q_v flux convergence in the mixed-phase layer (plus the q_v source due to large-scale advection) becomes smaller than the ice deposition rate at that level, remaining liquid quickly evaporates. In simulations with conversion to all-ice cloud this generally occurs within the first 6 h of integration. This process is somewhat similar to that discussed in Harrington et al. (1999) and Luo et al. (2008b).

To further illustrate how interactions between microphysics, radiation, and dynamics impact cloud phase, timeseries of various horizontally-averaged quantities for the LOWNI, HIGHNI, and BASE runs using DHARMA are shown in Fig. 14. For the LOWNI and BASE simulations that sustain liquid water (Fig. 14a), peak cloud top radiative cooling rates exceed 60 K day^{-1} over the duration of the simulations (Fig. 14c). In contrast, cloud top radiative cooling decreases steadily after approximately the first hour of integration in HIGHNI, corresponding with the decrease in LWP. In all three simulations, TKE increases during the first hour as the model dynamics spin up, but subsequently decreases in HIGHNI (Fig. 14d) with the loss of cloud top radiative cooling. The q_v flux convergence closely tracks the TKE, increasing during the first hour with model spinup and then decreasing thereafter in HIGHNI but remaining large in BASE and LOWNI (Fig. 14e). After spinup, the condensation rate closely follows the q_v flux convergence and decreases after the first hour in HIGHNI, falling to zero by $t = 6$ h (1800 UTC) (Fig. 14g). Ice deposition rates show a near-linear scaling with N_{IN} prior to the disappearance of liquid water (Fig. 14e). Ice growth is maintained in HIGHNI even after the (resolved and sub-grid) q_v flux convergence decreases to near zero because of moistening from the large-scale advective forcing. Overall, these results suggest close coupling between liquid water, cloud top radiative cooling, and cloud dynamics.

An analysis of the q_i budget indicates that ice deposition is the primary source for q_i in the mixed-phase layer in all of the simulations (for example, it is about 2–4 times larger than the combined effects of droplet freezing and riming for DHARMA). The ice deposition rate near the start of the simulations is much smaller than the condensation rate and q_v flux convergence (about an order of magnitude smaller in DHARMA for HIGHNI, with even greater differences for LOWNI and BASE). However, the larger ice deposition rates in HIGHNI (in conjunction with droplet freezing and riming) are sufficient to set in motion a chain of events through the aforementioned interaction pathways that leads to rapid dissipation of liquid water. In general, domain-mean ice deposition rates exceeding roughly 1–2 $\times 10^{-5}$ g kg^{-1} s^{-1} appear to be large enough to promote glaciation in the simulations, although we emphasize that this threshold is likely to vary for different conditions, such as the surface and large-scale forcing. We note that since the system appears to be fairly close to important thresholds that cause collapse, perturbations to other parameters such as large-scale forcing might also induce rapid transition from the mixed-phase to all-ice cloud through the aforementioned feedback mechanisms.

Rapid collapse of the mixed-phase cloud layer through interactions between the microphysics, precipitation, radiation, and dynamics is broadly reminiscent of simulations indicating collapse of marine stratocumulus (Ackerman et al. 1993) or rapid thinning and transition from closed to open cell dynamics (Savic-Jovcic and Stevens 2008; Wang and Feingold 2009) with a reduction of CCN or droplet concentration. However, there are important differences between the present study and the transition of warm marine stratocumulus simulated in previous studies. In particular, precipitation and associated sub-cloud evaporation play a key role in cloud-scale and mesoscale circulations that drive the transition to open cells in marine stratocumulus (Savic-Jovcic and Stevens 2008; Wang and Feingold 2009). Here, sublimation of ice precipitation is limited or absent because of large differences in equilibrium vapor pressure between liquid and ice, meaning that the sub-cloud environment is ice supersaturated for some distance below cloud base, while ice grows rapidly by deposition in the cloud layer because of the large ice supersaturation. This provides an important sink for water vapor and contrasts with the growth of drizzle drops through collision-coalescence in warm clouds. There are also other important

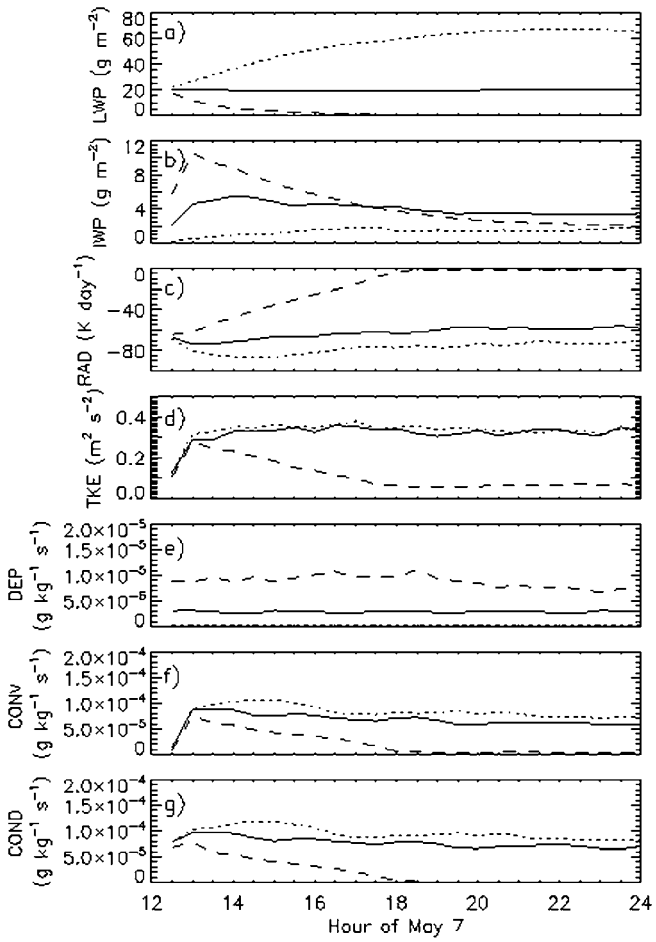

Figure 14. Timeseries of horizontally-averaged a) LWP, b) IWP, c) maximum cloud top radiative cooling rate in the vertical, RAD, d) TKE at a height of ~ 200 m, e) ice deposition rate, DEP, e) resolved and subgrid q_v flux convergence, CONV, and f) maximum droplet condensation rate in the vertical, COND, for the BASE (solid), LOWNI (dotted), and HIGHNI (dash) simulations from DHARMA. Presented DEP and CONV values are those at the level of maximum condensation rate.

differences such as the magnitude of the surface turbulent heat fluxes and the cold and dry Arctic free troposphere which allows for particularly efficient cooling of clouds through longwave emission.

In summary, ice deposition does not by itself lead to glaciation of the cloud as shown by budget analysis. However, it does appear to play an important *indirect* role through interactions with the surface precipitation flux, radiation, and dynamics. The timescale for spin-up of the BL dynamics may also be important for determining whether or not the mixed-phase cloud is maintained. In our simulations, ice is introduced at the start of the integrations following the approach of the M-PACE model intercomparison (Klein et al. 2009; Morrison et al. 2009a). One might anticipate that in simulations with enhanced ice deposition such as HIGHNI, liquid water could be reduced rapidly enough that significant cloud motion fails to spin up. This could enhance sensitivity to the ice deposition rate and hence N_{IN}. Timeseries of the resolved TKE suggest that the dynamics are relatively well-developed in many, but not all, of the simulations prior to dissipation of liquid, with TKE subsequently decreasing in simulations with conversion to all-ice cloud (as shown for DHARMA in Fig. 14d). Sensitivity tests with ice introduced only after the cloud dynamics are fully-developed would address this issue and should be considered in future mixed-phase BL cloud intercomparison studies.

7. Discussion and conclusions

An intercomparison of simulations of an Arctic mixed-phase BL stratus observed during SHEBA/FIRE-ACE using six LES and cloud resolving models was presented. Limited riming, aggregation, and ice crystal sublimation reduce microphysical complexity and make this case well-suited for model intercomparison. Initial conditions and large-scale forcing were based on observations and analysis data, but modified to minimize drift in the thermodynamic fields above the BL.

A unique aspect of this study is that the diagnostic concentration of ice nuclei, N_{IN}, was specified in all models

in a way that held the concentration of crystals, N_i, approximately fixed during the simulations. Thus, sensitivity to N_{IN} in this context was analogous to sensitivity to N_i. This procedure was used to minimize large differences in the treatment of ice nucleation between the models that might otherwise dominate the results. The baseline simulations specified $N_{IN} = 1.7\ \mathrm{L}^{-1}$, based on the average CFDC IN concentration observed above the BL sampled at in-cloud conditions of temperature and supersaturation and suggestions that N_i is often roughly similar to above-cloud IN concentrations (Prenni et al. 2009). Sensitivity tests were run for each model with N_{IN} set to $0.17\ \mathrm{L}^{-1}$ (LOWNI) or $5.1\ \mathrm{L}^{-1}$ (HIGHNI).

The baseline simulations differed widely in terms of liquid and ice water paths and radiative fluxes, broadly consistent with the previous M-PACE intercomparison of Arctic mixed-phase BL stratocumulus (Klein et al. 2009). Assuming baseline N_{IN}, most but not all models simulated a persistent mixed-phase cloud qualitatively similar to what was observed. Results were highly sensitive to N_{IN}; larger N_{IN} led to rapid transition from mixed-phase to all-ice clouds in five of the six models. This supports many previous modeling studies indicating strong sensitivity of Arctic mixed-phase clouds to N_{IN} or N_i (e.g., Pinto 1998; Harrington et al. 1999; Jiang et al. 2000; Morrison et al. 2003; Morrison et al. 2005a; Prenni et al. 2007; Solomon et al. 2009; Avramov and Harrington 2010). We emphasize that in contrast to the diagnostic approach for IN employed here and in many previous modeling studies, using a prognostic approach for IN means that N_i can diverge from the initial IN concentration. In some modeling studies of Arctic mixed-phase clouds that utilized a prognostic IN concentration, N_i rapidly decreased over time as the IN were consumed and depleted, thereby reducing sensitivity to the initial IN concentration (Harrington and Olson 2001; Morrison et al. 2005a; Fridlind et al. 2011). However, a difficulty in prognosing IN is that sources of IN and specific mechanisms controlling nucleation in mixed-phase clouds remain highly uncertain (Fridlind et al. 2007; Fan et al. 2009).

All baseline and sensitivity simulations clustered into two quasi-steady states associated with either persistent mixed-phase clouds or all-ice clouds after the first few hours of integration, implying the existence of multiple states for this case. These two states were associated with distinctly different microphysical, thermodynamic, and radiative characteristics. Simulations with persistent mixed-phase clouds had larger surface downwelling LW and smaller SW fluxes, greater rates of cloud top radiative cooling, and more vigorous vertical transport and mixing within the BL, compared to simulations with rapid glaciation and conversion to all-ice clouds. While not the subject of this study, these large differences in radiative and BL characteristics between the two states would be expected to have a large impact on the surface energy budget and hence evolution of sea ice.

A key point is that this bifurcation of solutions occurred using different models subject to the same initial and forcing conditions and N_{IN}, or using the same model with small changes to N_{IN}. This led to rapid divergence of solutions along different trajectories leading to either the mixed-phase or all-ice state and large spread of model results. However, we emphasize that simulations producing a given state were similar regardless of the particular model or specification of N_{IN}. Bifurcation of solutions also may point to limits on short-term (i.e., hours to a few days) predictability of the system state; future work is needed to characterize the response to small perturbations in a more systematic framework.

Persistent mixed-phase clouds appeared to be largely self-maintained in the simulations through interactions with radiation and dynamics. Significant liquid water in these simulations led to large rates of cloud top radiative cooling. This in turn led to stronger vertical transport and mixing that helped to sustain droplet condensation. The amount of liquid water required to maintain the cloud through this feedback mechanism is unclear, and likely to vary from case to case; this is left as a subject of future work. Previous studies have also suggested the important role of cloud dynamics in maintaining mixed-phase clouds (Mazin 1986; Rauber and Tokay 1991; Harrington et al. 1999; Korolev and Isaac 2003; Korolev 2008; Korolev and Field 2008). For example, Korolev (2008) and Korolev and Field (2008) examined dynamical conditions supporting persistent mixed-phase clouds using an oscillating parcel model with specified dynamical characteristics. They quantified minimum updraft velocities and vertical extents required to support liquid for various N_i and rates of ice deposition.

Here, changes in ice deposition rate between simulations with persistent liquid water and those with conversion to all-ice were generally much smaller than changes in the condensation rate within the mixed-phase layer. Thus, changes in ice deposition rate associated with modification of N_{IN} had a fairly limited *direct* impact on glaciation of liquid water. However, ice deposition appeared to play a key *indirect* role through several interaction pathways involving changes in the surface precipitation flux, cloud top radiative cooling, and cloud dynamics, leading to rapid glaciation and conversion to all-ice cloud. A mean ice deposition rate in the mixed-phase layer greater than about $1\text{–}2 \times 10^{-5}\ \mathrm{g\ kg^{-1}\ s^{-1}}$ appeared to be sufficient to promote rapid glaciation in most models. We emphasize that this threshold is likely to vary for different cases and conditions such as the surface and large-scale forcing. Our results suggest the critical importance of these interaction pathways in determining cloud phase, which have been neglected in the fixed dynamical parcel studies of Korolev (2008) and Korolev and Field (2008). Since depositional growth rates for crystals of various size and habit remain highly uncertain (Chen and Lamb 1994; Nelson and Baker 1996; Wood et al. 2001; Avramov and Harrington 2010), our results also suggest the

need for better observational characterization of depositional growth and its parameterization in models. Future work using fully dynamical models in conjunction with a specified kinematic flow field model (e.g., Kinematic Driver Model, KiD; Shipway and Hill 2010) should be able to further quantify the role of microphysical-radiative-dynamical feedbacks versus microphysical processes alone in determining cloud phase. We note that these feedbacks may be less important for cases in which there is a significant surface component to the buoyant production of kinetic energy, such as in the cold-air outbreak during M-PACE.

The diagnostic approach for IN utilized here was a major simplification, since this meant that N_i was essentially held fixed during the simulations; spatial and temporal variability of N_i for the real cloud system observed during this case was indicated by in-situ observations for particles larger than 100 μm (Morrison et al. 2011), as well as inferred from radar reflectivity (Fridlind et al. 2011). Retrievals have suggested more generally that IWP is positively correlated with LWP for Arctic low-level mixed-phase clouds (Shupe et al. 2008), and that ice nucleation tends to be associated with the presence of liquid water (Morrison et al. 2005a; de Boer et al. 2011). Studies have hypothesized that direct links between ice nucleation and liquid droplets might result from ice nucleation that primarily occurs through contact freezing (Morrison et al. 2005a), immersion freezing (de Boer et al. 2010), or evaporation freezing (Fridlind et al. 2007). However, direct observational evidence supporting these modes of nucleation is far from sufficient.

The key point is that if ice nucleation is directly dependent on the droplet characteristics (e.g., droplet size), this could represent an important negative feedback whereby ice nucleation and hence ice deposition are reduced as liquid water dissipates. Such a negative feedback would help to counter the interaction pathways identified here that accelerate glaciation, and thus could help to sustain mixed-phase clouds. This effect was not investigated in the current study, but should be explored in future work. Progress will ultimately require development of new techniques to isolate and measure ice nuclei acting in various modes that are difficult or impossible to measure with current instrumentation.

In future work, we plan to follow up the current study with an intercomparison of models for a case of mixed-phase BL stratus observed during the 2008 ISDAC experiment (McFarquhar et al. 2011). There were improved observations of aerosols and ice crystals during ISDAC relative to SHEBA/FIRE-ACE. We also plan to further explore the parameter space that determines evolution of cloud phase in models, including extension to additional parameters not considered in the present study such as horizontal and vertical grid spacing.

The simplicity of the present case makes it well-suited for studies of mixed-phase cloud processes. It has served as the basis for at least three additional modeling efforts (Fridlind et al. 2011; de Boer et al. 2011; 2010). The current paper documents this case and presents simulations from several different models. This effort adds to the list of benchmark Arctic mixed-phase case studies (along with M-PACE, and expected in the near future, ISDAC). We hope that it will continue to be utilized in future studies.

Acknowledgments: We thank our colleagues in the SHEBA Atmospheric Surface Flux Group, E. Andreas, C. Fairall, P. Guest, and P. O. Persson, for collecting and processing the SHEBA surface data, and R. Moritz for the SHEBA sonde data. We also thank M. Shupe and B. van Deidenhoven for helpful discussions. HM was supported by U.S. DOE ARM DE-FG02-08ER64574 and the NSF Science and Technology Center for Multiscale Modeling of Atmospheric Processes (CMMAP), managed by Colorado State University under cooperative agreement ATM-0425247. GB acknowledges NASA (NNX07AQ81G) and the US DOE (ER64187-1027586-0011923) for funding support. Lawrence Berkeley National Laboratory is managed by the University of California under US DOE grant DE-AC02-05CH11231. JF and MO were supported primarily by the U.S. DOE Atmospheric System Research, an Office of Science, Office of Biological and Environmental Research (OBER) program; the Pacific Northwest National Laboratory is operated for the DOE by Battelle under contract DE-AC05-76RLO-1830. ASA and AMF were supported by the DOE Office of Science, OBER, through Interagency Agreements DE-AI02-06ER64173 and DE-AI02-08ER64527, the DOE National Energy Research Scientific Computing Center, and the NASA Radiation Sciences Program and Advanced Supercomputing Division. PZ was supported by NASA Interdisciplinary Studies grant NNG04G171G. JYH would like to thank the National Science Foundation for support under Grants ATM-0639542 and AGS-0951807 and The Department of Energy Atmospheric Systems Research Program for support under Grants DE-FG02-05ER64058 and DE-FG02-08ER4570. YL was supported by the National Natural Science Foundation of China (projects 40875064 and 40921003), the Basic Research Fund of the Chinese Academy of Meteorological Sciences (2007R001), and the Special Fund for Research in Meteorology (GYHY200806020). TH was supported by NASA (NNX07AQ81G).

References

Ackerman, A. S., O. B. Toon, and P. V. Hobbs, 1993: Dissipation of marine stratiform clouds and collapse of the marine boundary layer due to the depletion of cloud condensation nuclei by clouds. *Science*, **262**, 226–229, doi: 10.1126/science.262.5131.226.

Ackerman, A. S., P. V. Hobbs, and O. B. Toon, 1995: A model for particle microphysics, turbulent mixing, and radiative transfer in the stratocumulus-topped marine boundary layer and comparisons with measurements. *J. Atmos. Sci.*, **52**, 1204–1236, doi: 10.1175/1520-0469(1995)052<1204:AMFPMT>2.0.CO;2.

Ackerman, A. S., M. P. Kirkpatrick, D. E. Stevens, and O. B. Toon, 2004: The impact of humidity above stratiform clouds on indirect aerosol climate forcing. *Nature*, **432**, 1014–1017, doi: 10.1038/nature03174.

Ackerman, T. P. and G. Stokes, 2003: The Atmospheric Radiation Measurement program. *Physics Today*, **56**, 38–45, doi: 10.1063/1.1554135.

Avramov, A., and J. Y. Harrington, 2010: Influence of parameterized ice habit on simulated mixed phase Arctic clouds. *J. Geophys. Res.*, **115**, D03205, doi: 10.1029/2009JD012108.

Bigg, E., and C. Leck, 2001: Cloud active particles over the central Arctic Ocean. *J. Geophys. Res.*, **106**, 32155–32166, doi: 10.1029/1999JD901152.

Bretherton, C. S., and Coauthors, 1999: An intercomparison of radiatively driven entrainment and turbulence in a smoke cloud as simulated by different numerical models. *Q. J. Roy. Meteor. Soc.*, **125**, 391–423, doi: 10.1002/qj.49712555402.

Chen, J.-P., and D. Lamb, 1994: The theoretical basis for the parameterization of ice crystal habits: Growth by vapor deposition. *J. Atmos. Sci.*, **51**, 1206–1221, doi: 10.1175/1520-0469(1994)051<1206:TTBFTP>2.0.CO;2.

Cotton, W. R. and Coauthors, 2003: RAMS 2001: Current status and future directions. *Meteor. Atmos. Phys.*, **82**, 5–29, doi: 10.1007/s00703-001-0584-9.

Curry, J. A., W. B. Rossow, D. Randall, and J. L. Schramm, 1996: Overview of Arctic cloud and radiation characteristics. *J. Clim.*, **9**, 1731–1764, doi: 10.1175/1520-0442(1996)009<1731:OOACAR>2.0.CO;2.

Curry, J. A., J. O. Pinto, T. Benner, and M. Tschudi, 1997: Evolution of the cloudy boundary layer during the autumnal freezing of the Beaufort Sea, *J. Geophys. Res.*, **102**, 13851–13860, doi: 10.1029/96JD03089.

Curry, J. A. and Coauthors, 2000: FIRE Arctic Clouds Experiment. *Bull. Amer. Met. Soc.*, **81**, 5–29, doi: 10.1175/1520-0477(2000)081<0005:FACE>2.3.CO;2.

de Boer, G., H. Morrison, M. D. Shupe, and R. Hildner, 2011: Evidence of liquid dependent ice nucleation in high-latitude stratiform clouds from surface remote sensors. *Geophys. Res. Lett.*, **38**, L01803, doi: 10.1029/2010GL046016.

de Boer, G., T. Hashino, and G. J. Tripoli, 2010: Ice nucleation through immersion freezing in mixed-phase stratiform clouds: Theory and numerical simulations. *Atmos. Res.*, **96**, 315–324, doi: 10.1016/j.atmosres.2009.09.012.

J. Fan, M. Ovtchinnikov, J. M. Comstock, S. A. McFarlane, A. Khain. 2009: Ice formation in Arctic mixed-phase clouds: Insights from a 3-D cloud-resolving model with size-resolved aerosol and cloud microphysics. *J. Geophys. Res.*, **114**, D04205, doi: 10.1029/2008JD010782.

Ferrier, B., 1994: A double-moment multiple-phase four-class bulk ice scheme. Part I: Description. *J. Atmos. Sci.*, **51**, 249–280, doi: 10.1175/1520-0469(1994)051<0249:ADMMPF>2.0.CO;2.

Fridlind, A. M. and Coauthors, 2007: Ice properties of single-layer stratocumulus during the Mixed-Phase Arctic Cloud Experiment (M-PACE): Part II. Model results. *J. Geophys. Res.*, **112**, D24202., doi: 10.1029/2007JD008646

Fridlind, A. M., B. van Diedenhoven, A. S. Ackerman, A. Avramov, A. Mrowiec, H. Morrison, P. Zuidema, and M. D. Shupe, 2011: A FIRE-ACE/SHEBA case study of mixed-phase Arctic boundary-layer clouds: Entrainment rate limitations on rapid primary ice nucleation processes. *J. Atmos. Sci.,* submitted.

Han, Y. and E. R. Westwater, 1995: Remote sensing of tropospheric water vapor and cloud liquid water by integrated ground-based sensors. *J. Atmos. Oceanic Technol.*, **12**, 1050–1059, doi: 10.1175/1520-0426(1995)012<1050:RSOTWV>2.0.CO;2.

Harrington, J. Y., T. Reisen, W. R. Cotton, and S. M. Kreidenweis, 1999: Cloud resolving simulations of Arctic stratus. Part II: Transition-season clouds. *Atmos. Res.*, **51**, 45–75, doi: 10.1016/S0169-8095(98)00098-2.

Harrington, J. Y., and P. Q. Olson, 2001: On the potential influence of ice nuclei on surface-forced marine stratocumulus cloud dynamics. *J. Geophys. Res.*, **106**, 27473–27484, doi: 10.1029/2000JD000236.

Hashino, T. and G. J. Tripoli, 2007: The spectral ice habit prediction system (SHIPS). Part I: Model description and simulation of vapor deposition process. *J. Atmos. Sci.*, **64**, 2210–2237, doi: 10.1175/JAS3963.1.

Hashino, T., and G. Tripoli, 2008: The spectral ice habit prediction systems (SHIPS): Simulation of nucleation and depositional growth of polycrystals. *J. Atmos. Sci.*, **65**, 3071–3094, doi: 10.1175/2008JAS2615.1.

Intrieri, J. M., M. D. Shupe, T. Uttal, and B. J. McCarty, 2002: An annual cycle of Arctic cloud characteristics observed by radar and lidar at SHEBA, *J. Geophys. Res.*, **107**, 8030, doi: 10.1029/2000JC000423.

Jiang, H. and Coauthors, 2000: Cloud resolving simulations of mixed-phase Arctic stratus observed during BASE: Sensitivity to concentration of ice crystals and large-scale heat and moisture advection. *J. Atmos. Sci.*, **57**, 2105–2117, doi: 10.1175/1520-0469(2000)057<2105:CRSOMP>2.0.CO;2.

Key, J., 2001: *Streamer* User's Guide, Cooperative Institute for Meterological Satellite Studies, University of Wisconsin, 96pp.

Khain, A., A. Pokrovsky, M. Pinsky, A. Seifert, and V. Phillips, 2004: Simulation of effects of atmospheric aerosols on deep turbulent convective clouds using a spectral microphysics mixed-phase cumulus cloud model. Part I: Model description and possible application. *J. Atmos. Sci.*, **61**, 2963–2982, doi: 10.1175/JAS-3350.1.

Khairoutdinov, M. F., and D. A. Randall, 2003: Cloud-resolving modeling of the ARM summer 1997 IOP: Model formulation, results, uncertainties and sensitivities.

J. Atmos. Sci., **60**, 607–625, doi: 10.1175/1520-0469(2003)060<0607:CRMOTA>2.0.CO;2.

Klein, S., and Coauthors, 2009: Intercomparison of model simulations of mixed-phase clouds observed during the ARM Mixed-Phase Arctic Cloud Experiment. Part I: Single layer cloud. *Quart. J. Roy. Meteor. Soc.*, **135**, 979–1002, doi: 10.1002/qj.416.

Korolev, A. V. and G. A. Isaac, 2003: Phase transformation in mixed-phase clouds. *Quart. J. Roy. Meteor. Soc.*, **129**, 19–38, doi: 10.1256/qj.01.203.

Korolev, A. V. and Coauthors, 2003: Observations of the microphysical structure of mixed-phase clouds. *Quart. J. Roy. Meteor. Soc.*, **129**, 39–66, doi: 10.1256/qj.01.204.

Korolev, A., 2007: Limitations of the Wegener–Bergeron–Findeisen Mechanism in the evolution of mixed-phase clouds. *J. Atmos. Sci.*, **64**, 3372–3375, doi: 10.1175/JAS4035.1.

Korolev, A. V. and P. R. Field, 2008: The effect of dynamics on mixed-phase clouds: Theoretical considerations. *J. Atmos. Sci.*, **65**, 66–86, doi: 10.1175/2007JAS2355.1.

Krueger, S., 1988: Numerical simulation of tropical cumulus clouds and their interaction with the subcloud layer. *J. Atmos. Sci.*, **45**, 2221–2250, doi: 10.1175/1520-0469(1988)045<2221:NSOTCC>2.0.CO;2.

Lawson, R. P. and P. Zuidema, 2009: Aircraft Microphysical and Surface-based Radar Observations of Summertime Arctic Clouds, *J. Atmos. Sci.*, **66**, 3505–3529, doi: 10.1175/2009JAS3177.1.

Luo, Y., K.-MXu, H. Morrison, and G. McFarquhar, 2008a: Arctic mixed-phase clouds simulated by a cloud-resolving model: Comparison with ARM observations and sensitivity to microphysics parameterizations. *J. Atmos. Sci.*, **65**, 1285–1303, doi: 10.1175/2007JAS2467.1.

Luo, Y., K.-MXu, H. Morrison, G. M. McFarquhar, Z. Wang, and G. Zhang, 2008b: Multi-layer arctic mixed-phase clouds simulated by a cloud-resolving model: Comparison with ARM observations and sensitivity experiments. *J. Geophys. Res.*, **113**, D12208, doi: 10.1029/2007JD009563.

Mazin, I. P., 1986: Relation of cloud phase structure to vertical motion. *Sov. Meteor. Hydrol.*, 27–35.

McFarquhar, G., and Coauthors, 2011: Indirect and Semi-Direct Aerosol Campaign (ISDAC): The impact of Arctic Aerosols on Clouds. *Bull. Amer. Meteor. Soc.*, **92**, 183–201

Meyers, M. P., R. L. Walko, J. Y. Harrington, and W. R. Cotton, 1997: New RAMS cloud microphysics prameterization. Part II: The two-moment scheme. *Atmos. Res.*, **45**, 3–39, doi: 10.1016/S0169-8095(97)00018-5.

Mitchell, D. L., R. Zhang, and R. L. Pitter, 1990: Mass-dimensional relationships for ice particles and the influence of riming on snowfall rates. *J. Appl. Meteor.*, **29**, 153–163, doi: 10.1175/1520-0450(1990)029<0153:MDRFIP>2.0.CO;2.

Moeng, C.-H., and Coauthors, 1996: Simulation of a stratocumulus-topped PBL: Intercomparison among different numerical codes. *Bull. Amer. Meteor. Soc.*, **77**, 261–278, doi: 10.1175/1520-0477(1996)077<0261:SOASTP>2.0.CO;2.

Morrison, H., M. D. Shupe, and J. A. Curry, 2003: Modeling clouds observed at SHEBA using a bulk microphysics parameterization implemented into a single-column model. *J. Geophys. Res.*, **108**, 4255, doi: 10.1029/2002JD002229.

Morrison, H., and J. O. Pinto, 2004: A new approach for obtaining advection profiles: Application to the SHEBA column. *Mon. Wea. Rev.,* **132**, 687–702, doi: 10.1175/1520-0493(2004)132<0687:ANAFOA>2.0.CO;2.

Morrison, H., M. D. Shupe, J. O. Pinto, and J. A. Curry, 2005a: Possible roles of ice nucleation mode and ice nuclei depletion in the extended lifetime of Arctic mixed-phase clouds. *Geophys. Res. Lett.,* **32,** L18801, doi: 10.1029/2005GL023614.

Morrison, H., J. A. Curry, and V. I. Khvorostyanov, 2005b: A new double-moment microphysics parameterization for application in cloud and climate models. Part I: Description. *J. Atmos. Sci.*, **62**, 1665–1677, doi: 10.1175/JAS3446.1.

Morrison, H., and J. O. Pinto, 2005: Mesoscale modeling of springtime arctic mixed-phase clouds using a new two-moment bulk microphpysics scheme. *J. Atmos. Sci***62**, 3683–3704, doi: 10.1175/JAS3564.1.

Morrison, H., and J. O. Pinto, 2006: Intercomparison of bulk microphysics schemes in mesoscale simulations of springtime Arctic mixed-phase stratiform clouds. *Mon. Wea. Rev.,* **134**, 1880–1900, doi: 10.1175/MWR3154.1.

Morrison, H. and Coauthors, 2009a: Intercomparison of model simulations of mixed-phase clouds observed during the ARM Mixed-Phase Arctic Cloud Experiment. Part II: Multi-layer cloud. *Quart. J. Roy. Meteor. Soc.*, **135**, 1003–1019, doi: 10.1002/qj.415.

Morrison, H., G. Thompson, M. Gilmore, W. Gong, R. Leaitch, and A. Muhlbauer, 2009b: WMO International Cloud Modeling Workshop. *Bull. Amer. Meteor. Soc.*, **90**, 1683–1686, doi: 10.1175/2009BAMS2817.1.

Morrison, H., G. Thompson, and V. Tatarskii, 2009c: Impact of cloud microphysics on the development of trailing stratiform precipitation in a simulated squall line: Comparison of one- and two-moment schemes. *Mon. Wea. Rev.,* **137**, 991–1007, doi: 10.1175/2008MWR2556.1.

Morrison, H., P. Zuidema, G. McFarquhar, A. Bansemer, and A. J. Heysmfield, 2011: Snow microphysical observations in shallow mixed-phase and deep frontal Arctic cloud systems. *Q. J. Roy. Meteor. Soc.* (in press)

Nelson, J., and M. B. Baker, 1996: New theoretical framework for studies of vapor growth and sublimation of small ice crystals in the atmosphere. *J. Geophys. Res.*, **101**, 7033–7047, doi: 10.1029/95JD03162.

Pinto, J. O., 1998: Autumnal mixed-phase cloudy boundary layers in the Arctic. *J. Atmos. Sci.*, **55**, 2016–2038, doi: 10.1175/1520-0469(1998)055<2016:AMPCBL>2.0.CO;2.

Prenni, A. J. and Coauthors, 2007: Can ice-nucleating aerosols affect Arctic seasonal climate? *Bull. Amer. Met. Soc.*, **88**, 541–550, doi: 10.1175/BAMS-88-4-541.

Prenni, A., P. De Mott, D. Rogers, S. Kreidenweis, G. McFarquhar, G. Zhang, and M. Poellot, 2009: Ice nuclei characteristics from m-pace and their relation to ice formation in clouds, *Tellus*,**61B**, 436–448.

Randall, D. A. and Coauthors, 2003: Confronting models with data: The GEWEX Cloud Systems Study. *Bull. Amer. Met. Soc.*, **84**, 455–469, doi: 10.1175/BAMS-84-4-455.

Rauber, R., and A. Tokay, 1991: An explanation for the existence of supercooled water at the top of cold clouds, *J. Atmos. Sci.*, **48**, 1005–1023.

Randall, D. A., and D. G. Cripe, 1999: Alternative methods for specification of observed forcing in single-column models and cloud system models. *J. Geophys. Res.*, **104**, 24527–24545, doi: 10.1029/1999JD900765.

Rogers, D. C., P. J. DeMott, and S. M. Kreidenweis, 2001: Airborne measurements of tropospheric ice-nucleating aerosol particles in the Arctic spring. *J. Geophys. Res.*, **106**, 15053–15063, doi: 10.1029/2000JD900790.

Sandvik, A. and Coauthors 2007: Observed and simulated microphysical composition of Arctic clouds: Data properties and model validation. *J. Geophys. Res.*, **112**,, doi: 10.1029/2006JD007351

Savic-Jovcic, V., and B. Stevens, 2008: The structure and mesoscale organization of precipitating stratocumulus. *J. Atmos. Sci.*, **65**, 1587–1605, doi: 10.1175/2007JAS2456.1.

Shipway, B. J., and A. A. Hill, 2010: A 1D modelling framework for a microphysics intercomparison study: Part I. *Q. J. Roy. Meteor. Soc.* (in press)

Shupe, M. D., and J. M. Intrieri, 2004: Cloud radiative forcing of the Arctic surface: The influence of cloud properties, surface albedo, and solar zenith angle. *J. Clim.*, **17**, 616–628, doi: 10.1175/1520-0442(2004)017<0616:CRFOTA>2.0.CO;2.

Shupe, M. D., S. Y. Matrosov, and T. Uttal, 2006: Arctic mixed-phase cloud properties derived from surface-based sensors at SHEBA. *J. Atmos. Sci.*, **63**, 697–711, doi: 10.1175/JAS3659.1.

Shupe, M. D., P. Kollias, M. Poellot, and E. Eloranta, 2008: On deriving vertical air motions from cloud radar Doppler spectra. *J. Atmos. Ocean. Technol.*, **25**, 547–557, doi: 10.1175/2007JTECHA1007.1.

Shutts, G. J. and M. E. B. Gray, 1994: A numerical modelling study of the geostrophic adjustment process following deep convection. *Quart. J. Roy. Met. Soc.*, **120**, 1145–1178.

Solomon, A., H. Morrison, P. O. G. Persson, M. D. Shupe, and J.-WBao, 2009: Investigation of microphysical parameterizations of snow and ice in Arctic clouds during M-PACE through model- observation comparisons, *Mon. Wea. Rev.*, **137**, 3110–3128, doi: 10.1175/2009MWR2688.1.

Stevens, B. and Coauthors, 2005: Evaluation of large-eddy simulations via observations of nocturnal marine stratocumulus. *Mon. Wea. Rev.*, **133**, 1443–1462, doi: 10.1175/MWR2930.1.

Stroeve, J., M. M. Holland, W. Meier, T. Scambos, and M. Serreze, 2007: Arctic sea ice decline: Faster than forecast. *Geophys. Res. Lett.*, **34**, L09501, doi: 10.1029/2007GL029703.

Sun, Z. and K. Shine, 1994: Studies of the radiative properties of ice and mixed-phase clouds. *Quart. J. Roy. Meteor. Soc.*, **120**, 111–137, doi: 10.1002/qj.49712051508.

Tripoli, G. J., 1992: A non-hydrostatic mesoscale model designed to simulate scale interaction. *Mon. Wea. Rev.*, **120**, 1342–1359, doi: 10.1175/1520-0493(1992)120<1342:ANMMDT>2.0.CO;2.

Uttal, T. and Coauthors, 2002: Surface Heat Budget of the Arctic Ocean. *Bull. Amer. Met. Soc.*, **83**, 255–275, doi: 10.1175/1520-0477(2002)083<0255:SHBOTA>2.3.CO;2.

Verlinde, H. and Coauthors, 2007: The Mixed-Phase Arctic Cloud Experiment (M-PACE). *Bull. Amer. Met. Soc.*, **88**, 205–221, doi: 10.1175/BAMS-88-2-205.

Wang, H., and G. Feingold, 2009: Modeling mesoscale cellular structures and drizzle in marine stratocumulus. Part II: The microphysics and dynamics of the boundary region between open and closed cells. *J. Atmos. Sci.*, **66**, 3257–3275, doi: 10.1175/2009JAS3120.1.

Wang, J., H. Cole, D. Carlson, E. Miller, K. Beierle, A. Paukkunen, and T. Laine, 2002: Corrections of humidity measurement errors from the vaisala rs80 radiosonde - application to toga coare data. *J. Atmos. Oceanic Technol.*, **19**, 981–1002, doi: 10.1175/1520-0426(2002)019<0981:COHMEF>2.0.CO;2.

Wood, S. E., M. B. Baker, and D. Calhoun, 2001: New model for the vapor growth of hexagonal ice crystals in the atmosphere. *J. Geophys. Res.*, **106**, 4845–4870, doi: 10.1029/2000JD900338.

Yum, S. S., and J. G. Hudson, 2001: Vertical distributions of cloud condensation nuclei spectra over the springtime Arctic Ocean. *J. Geophys. Res.*, **106**, 15045–15052, doi: 10.1029/2000JD900357.

Zuidema, P. and Coauthors, 2005: An Arctic springtime mixed-phase cloudy boundary layer observed during SHEBA. *J. Atmos. Sci.*, **62**, 160–176, doi: 10.1175/JAS-3368.1.

Appendix -Description of the experimental setup

The initial profiles of liquid water potential temperature, θ_l, and total water, q_t, are assumed to be constant within the BL, with θ_l = 257 K (close to observations from the 2335 UTC sonde, see Fig. 3a), and q_t = 0.915 g kg^{-1}, corresponding to near-surface relatively humidity RH of 86%. Note that this gives RH within the BL up to 12% higher than observed (Fig. 3b), although the sonde measurements have been shown to exhibit a dry bias (Wang et al. 2002); this is suggested here by the maximum RH of ~ 95% from the 1730 and 2335 UTC sondes despite the presence of liquid water indicated by aircraft, lidar, and MWR. This value of initial q_t is derived from θ_l and the assumption of an adiabatic liquid cloud with a LWP of about 20 g m^{-2}. The

surface pressure, p_{sfc}, and inversion pressure level atop the BL, p_{inv}, are 101700 and 95700 Pa, respectively. At p_{inv}, $\theta_l = 263.9$ K (resulting in a temperature inversion of 6.1 K over a distance of 40 m) and $q_t = 0.8$ g kg^{-1}. Vertical gradients of θ_l and q_t above the inversion are chosen so that the change in these quantities due to vertical advection and compression heating associated with large-scale subsidence approximately balances the large-scale horizontal advective forcing (see below). The vertical gradients of θ_l and q_t above the BL are given by

$$\frac{d\theta_l}{dp} = \frac{\theta_l}{T}\min\left(3.631\times10^{-8}(95700-p), 0.00057\right), \quad 60000 < p < p_{inv} \tag{A1}$$

$$\frac{dq_t}{dp} = 1.4\times10^{-5}, 60000 < p < p_{inv} \tag{A2}$$

where p is air pressure in Pa. For $p < 60000$ Pa, θ_l and q_t profiles are obtained directly from the sonde. The initial profiles given by the approach described above, along with observations from the sondes launched at 1115, 1730, and 2335 UTC, are shown in Fig. 3.

The initial cloud is assumed to be composed entirely of liquid, with the liquid water mixing ratio consistent with θ_l and q_t assuming equilibrium (exactly saturated) conditions inside the cloud. The initial cloud base is located at $\sim$ 220 m with a vertical thickness of about 280 m. It was assumed that the models would generate ice after initialization and achieve a quasi-steady state in terms of microphysics.

Lower boundary conditions are based on observations from the Atmospheric Surface Flux Group tower at SHEBA (Persson et al. 2002), averaged from 1200 UTC to 2400 UTC 7 May. The surface latent and sensible turbulent heat fluxes are set to 2.86 and 7.98 W m^{-2}, respectively, where positive values are defined as a flux of heat from the surface to the atmosphere. The roughness length is assumed to be 4×10^{-4} m. For radiation, the surface is assumed to be ice-covered with a temperature of 257.4 K and broadband shortwave albedo of 0.827. Note that since surface heat fluxes are specified, the specified surface temperature only impacts longwave radiative transfer in the models. These values for the lower boundary condition are held fixed over the course of the simulations.

The large-scale forcings applied in the simulations are based on data from the European Center for Medium Range Weather Forecast (ECMWF) analysis constrained by SHEBA observations (Morrison and Pinto 2004), and further modified as described below. Note that since the large-scale forcing dataset is derived from analysis rather than directly from observations (such as provided by a sounding network), there is considerable uncertainty in these quantities. The analysis data applied to the models are averaged over the period from 1200 to 2400 UTC 7 May. Meridional and zonal winds from analysis are used to nudge model winds with a timescale of 1–2 h to prevent significant drift of the mean model wind. For the large-scale advective forcing, horizontal advective forcing is specified along with large-scale vertical pressure velocity, ω, which are used to calculate vertical advection using the predicted model profiles [following Eq. (6) in Randall and Cripe (1999)]. Within the BL ($p > p_{inv}$), the ECMWF data provide large-scale horizontal advective forcing of temperature and water vapor. Above the BL ($p < p_{inv}$), the large-scale forcing is idealized to give minimal drift of temperature and water vapor. The large-scale horizontal advective forcing of temperature (K s^{-1}) and water vapor (g kg^{-1} s^{-1}) for $p < p_{inv}$ is given by

$$\left(\frac{\partial T}{\partial t}\right)_{adv} = \min\left(1.815\times10^{-9}(95700-p), 2.85\times10^{-5}\right) - 0.05\frac{R_d T}{c_p p} \tag{A3}$$

$$\left(\frac{\partial q_v}{\partial t}\right)_{adv} = 7\times10^{-7}$$

where c_p is the specific heat of dry air at constant pressure and R_d is the gas constant for dry air. Large-scale vertical pressure velocity, ω, is specified to increase linearly with p from zero at p_{sfc} to 0.05 Pa s^{-1} at p_{inv} (0.05 Pa s^{-1} is the approximate cloud-top value form the ECMWF analyses, averaged from 1200 to 2400 UTC 7 May). At heights above p_{inv}, $\omega = 0.05$ Pa s^{-1}. The profiles of ω and large-scale horizontal advective forcing of T and q_v used to force the models are shown in Fig. A1.

Large-scale horizontal advective forcing of hydrometeors is neglected. Large-scale vertical advection of hydrometeors is based on the predicted model fields and specified ω. At heights above 70000 Pa, all model variables are held fixed during the integration.

Longwave and shortwave radiative transfer are calculated using each of the models' radiation codes and simulated thermodynamic and cloud fields. The solar zenith angle varies realistically as a function of the simulation time. Profiles of downwelling longwave and shortwave fluxes, which are used by models employing relatively low model lids (i.e., within in the troposphere), are derived using Streamer (Key 2001) at 45 m vertical spacing as detailed in Zuidema et al. (2005).

For models with coupling of cloud droplets to aerosols, CCN are derived approximately following condensation nuclei (CN) measurements described by Yum and Hudson (2001). Since no direct aerosol size or composition measurements were available, the aerosol specification is the same as for the M-PACE intercomparison, but with the total concentration adjusted to reflect the SHEBA/FIRE-ACE CN measurements. The aerosol is assumed to follow a bimodal lognormal size distribution. The size distribution for each mode is given by

$$\frac{dN}{d\ln r} = \frac{N_t}{\sqrt{2\pi}\ln\sigma}\exp\left[-\frac{\ln^2(r/r_m)}{2\ln^2\sigma}\right] \tag{5}$$

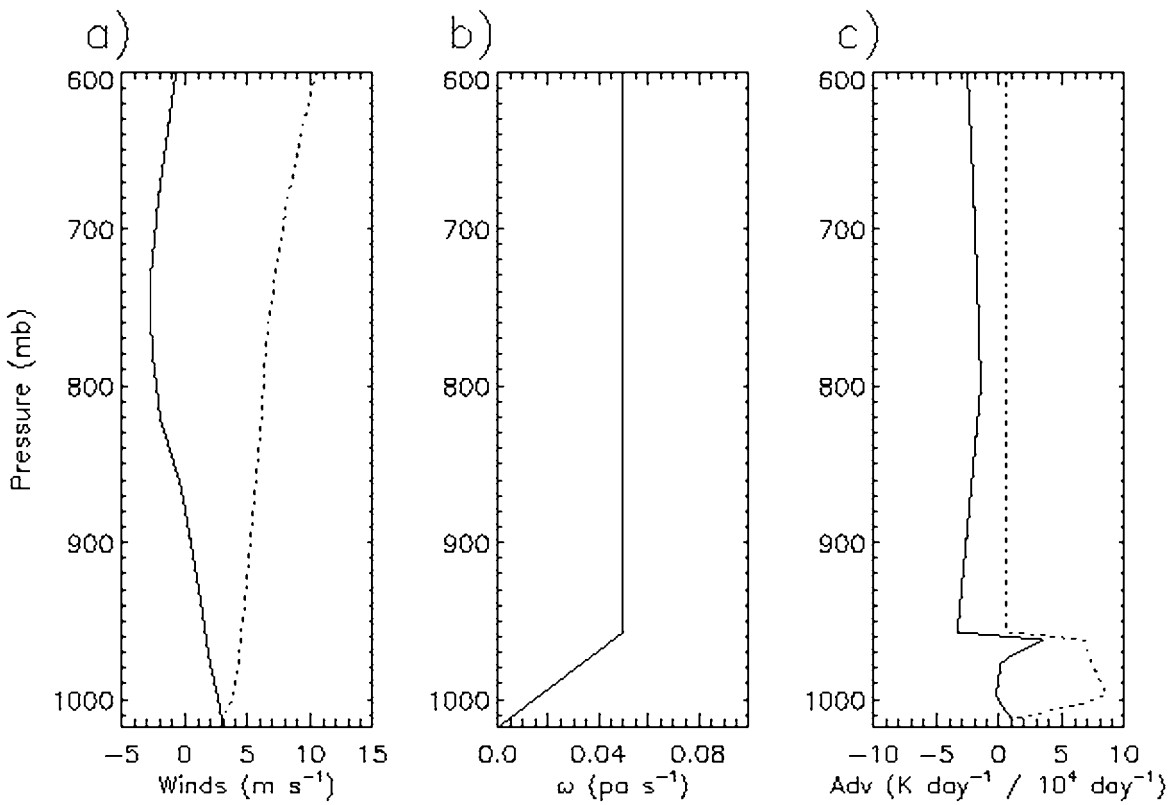

Figure A1. Large-scale forcing for the model simulations: a) zonal (solid) and meridional (dotted) winds, b) vertical pressure velocity, and c) horizontal advection of temperature (solid) and water vapor mixing ratio (dotted).

where r is aerosol radius. The aerosol parameters σ, r_m, and N_t are the geometric standard deviation, mean, and total number concentration of each mode, respectively. For mode 1 (smaller), these values are 2.04, 0.052 μm, and 350 cm^{-3}, respectively. For mode 2 (larger), these values are 2.5, 1.3 μm, and 1.8 cm^{-3}, respectively. Simulations using four of the models (DHARMA, UCLA-CAMS, SAM-SBM, UW-NMS) with aerosols modified to represent more pristine conditions as observed during M-PACE indicate limited sensitivity to CCN concentrations, relative to the sensitivity to IN. A possible reason for the lack of sensitivity is that ice nucleation in the simulations is specified as described in section 4, and thus is independent of droplet characteristics. Previous studies have suggested greater sensitivity of Arctic mixed-phase clouds to CCN may occur when ice nucleation occurs through liquid-dependent modes such as immersion freezing (e.g., de Boer et al. 2011; 2010).